Homogeneous steady deformation: A review of computational techniques

Joshua R. Davis[1], Sarah J. Titus[2*]

[1] *Department of Mathematics, Carleton College; jdavis@carleton.edu*

[2] *Department of Geology, Carleton College; *corresponding author; stitus@carleton.edu*

Abstract

Homogeneous steady models are frequently used in the structural geology community to describe rock deformation. We review the literature on these models in a streamlined, coordinate-free framework based on matrix exponentials and logarithms. These mathematical tools allow us to compute progressive and simultaneous deformations easily. As an application, we develop transpression with triclinic symmetry in two ways. The tools let us integrate field data related to position and velocity in computing best-fit models with many degrees of freedom. As an application, we reanalyze a published study to demonstrate the extent to which kinematic vorticity is sensitive to modeling assumptions. The tools also open the door to an increased role for the mathematics of Lie groups (spaces of deformations) in structural geology. We suggest two topics for further study: numerical methods for non-steady deformations, and statistics of deformation tensors.

Keywords: kinematic model, homogeneous deformation, velocity gradient, transpression, vorticity

1. Introduction

Natural rock deformation is neither homogeneous nor steady (e.g., Lister and Williams, 1983; Jiang and White, 1995). The rock experiencing deformation may be heterogeneous and anisotropic (e.g., Biot, 1961; Cobbold et al., 1971; Weijermars, 1992; Goodwin and Tikoff, 2002). The stress field may vary in space and time (e.g., Angelier et al., 1985; Bergerat, 1987; Zoback, 1992; Bird, 2002). Thermal and chemical conditions can change during deformation (e.g., Etheridge et al., 1983; Pavlis, 1986; Dunlap et al., 1997; Whitney et al., 2007).

Despite these complexities, many structural geologists use homogeneous, steady, purely kinematic models to analyze data from naturally deformed rocks. The primary justification for this simplification is that a scale can often be chosen on which the deformation is approximately homogeneous (e.g., Ramsay and Graham, 1970; Means, 1976; Ramsay and Huber, 1983; Twiss and Moores, 2007; Fossen, 2010). Further, homogeneous steady models can be combined to construct nonlinear models at other scales. For example, homogeneous steady models developed at different points in space may allow estimates of deformation partitioning (e.g., Law et al., 1984; Tikoff and Teyssier, 1994; Horsman and Tikoff, 2005; Sullivan and Law, 2007; Titus et al., 2011). Models developed at different points in time may constrain the deformation path (e.g., Elliott, 1972; Evans and Dunne, 1991; Grasemann et al., 1999; Mookerjee and Mitra, 2009; Weil et al., 2010). In contrast, dynamical models have the advantage of being based in physical law, but they are complicated. The simplest dynamical model of viscous fluid flow — the Navier-Stokes equations — is not well understood in theory (Fefferman, 2006). Field data are always incomplete, and they are often too scant to warrant a complicated model.

The earliest kinematic models in structural geology were based on the two-dimensional simple shear zone of Ramsay and Graham (1970). A major advantage of simple shear is that there is no slip along the shear zone boundary and therefore no strain compatibility issues across the zone. However, over time workers have recognized that simple shear is not rich enough to describe shear zones with significant flattening (e.g., Coward, 1976), regions with both vertical uplift and horizontal shearing (Sylvester and Smith, 1976), or patterns of folding (Sanderson and Marchini, 1984) in classic wrench tectonic terranes (Wilcox et al., 1973; Harding, 1973).

To account for such complexities, kinematic models have become three-dimensional and increasingly general. For instance, models for transpression/transtension with monoclinic symmetries have been developed (Sanderson and Marchini, 1984; Fossen and Tikoff, 1993; Simpson and De Paor, 1993) and applied to many field-based datsets (e.g., Ring, 1998; Bailey and Eyster, 2003; Baird and Hudleston, 2007; Titus et al., 2007; Vitale and Mazzoli, 2009). Transpressions with triclinic symmetry (Jones and Holdsworth, 1998; Lin et al., 1998; Iacopini et al., 2007) have been applied to a variety of tectonic problems (Czeck and Hudleston, 2003; Tavarnelli et al., 2004; Clegg and Holdsworth, 2005; Horsman et al., 2008; Sarkarinejad and Azizi, 2008). Some of these models include an added component of extrusion (Dias and Ribeiro, 1994; Xypolias and Koukouvelas, 2001; Neves et al., 2005; Wang et al., 2005;

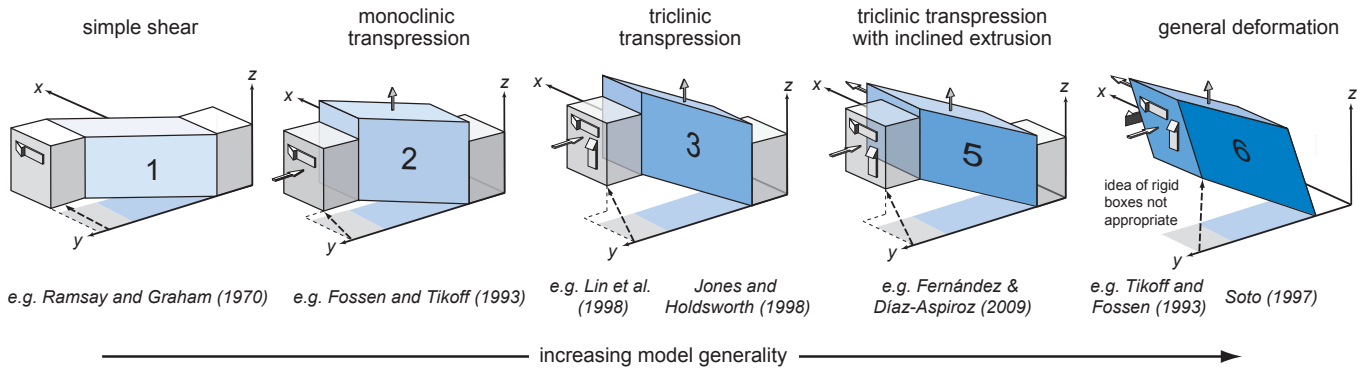

Figure 1: Over time, workers have employed increasingly rich deformation models. Each model is labeled with its number of degrees of freedom (not counting the three degrees of freedom implicit in choosing coordinates).

Sarkarinejad and Azizi, 2008; Fernández and Díaz-Azpiroz, 2009). Tikoff and Fossen (1993) and Soto (1997) introduced even more general models (see Appendix A), which have been applied to natural rock deformation only rarely (e.g., Yonkee, 2005).

Despite the different components of deformation included in particular kinematic models, the method of their construction is similar. One commonly begins with a velocity field and solves for the resulting finite deformation. This "forward" process is well understood in geology (e.g., Ramberg, 1975; Tikoff and Fossen, 1993; Lin et al., 1998). Unfortunately, geologic field data are often related not to the velocity field but to the finite deformation. To recover the velocity field, or to integrate data relating to both position and velocity, one must work "backward" from deformation to velocity.

Provost et al. (2004) introduced mathematical tools — matrix exponentials and logarithms — that expedite the "forward" and "backward" computations. While Provost et al. (2004) presented all of the requisite mathematics, they did not offer many explicit geological applications.

In this paper, we advance the previous work by applying the exponential/logarithm method to two major examples: a forward problem of constructing a new kinematic model of transpression (Section 3) and an inverse problem of finding the best homogeneous steady model for a given set of field data (Section 5). In service to the latter application, we review various kinds of geological data (e.g., paleomagnetic rotations, lineation directions), related to both velocity and position, and describe how they can be integrated into the computation of a best-fit model with many degrees of freedom (Section 4). We discuss the advantages of this approach and its connection to the mathematical theory of Lie groups (Section 6). This theory may be useful in developing further computational techniques for structural geology. We propose two ideas for further exploration: numerical methods for non-steady deformations, and statistics of deformation tensors. In an extensive appendix, we summarize the mathematical definitions, theorems, and algorithms, and compute a number of explicit geological examples.

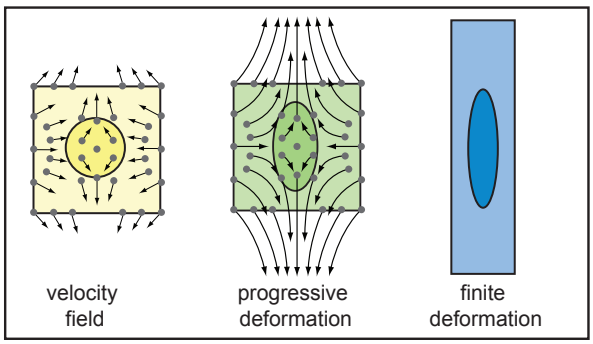

Figure 2: A velocity field determines a progressive deformation, which in turn determines a finite deformation.

2. Mathematical framework

Any rock deformation (or general fluid flow) can be described as a velocity vector field, which gives the velocity of each point particle in the rock at each instant during the deformation (Fig. 2). For reasons outlined in Section 1, in structural geology the velocity field is often assumed to be *homogenous* and *steady* — that is, to satisfy the differential equation

$$\dot{\vec{y}} = L\vec{y}, \tag{1}$$

where $\vec{y}$ is position, the dot denotes differentiation with respect to time t, and L is a constant real tensor called the *velocity gradient tensor*.

In addition to the velocity field, two other concepts are useful for describing rock deformation (Fig. 2). The *progressive deformation* describes the path of each particle in the deforming rock over time. The *finite deformation* describes the net effect of the deformation between its starting and ending times. Computing these quantities amounts to solving the differential equation. The form of solution that we favor in this paper is

$$\vec{y} = (\exp tL)\vec{x}, \tag{2}$$

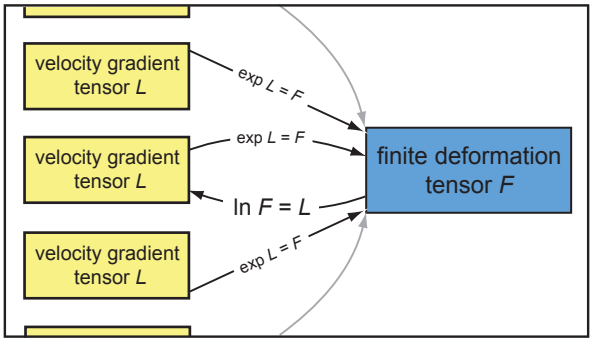

Figure 3: The tensor L that describes the velocity field exponentiates to the tensor F that describes finite deformation. The tensor F may have multiple such logarithms, but there is a principal logarithm $\ln F$ of special importance.

where $\vec{x}$ is any initial position and exp denotes the matrix exponential function (see Appendix B and Passchier (1988b)). We assume that the time scale is chosen so that t runs from 0 to 1. The finite deformation is then $\vec{y} = F\vec{x}$, where

$$F = \exp L$$

is the *finite deformation tensor* or *position gradient tensor* that relates initial positions $\vec{x}$ to final positions $\vec{y}$.

Because $F = \exp L$, it is tempting to write $L = \ln F$. This statement requires care, because some matrices do not have real logarithms, while others have infinitely many. Fortunately, for the finite deformation tensors F that commonly arise in structural geology, a well-defined real *principal logarithm* $\ln F$ exists (see Fig. 3 and Appendix C).

In the cases when the finite deformation tensor F has more than one real logarithm, selecting $L = \ln F$ leads to a "simplest" progressive deformation that explains F. By "simplest" we mean the one with the least rigid rotation. In analysis of deformed rock, this choice may or may not be the true deformation, but it serves as a useful starting point, especially when rotation cannot be characterized from the field data. Fig. 4 shows an explicit example. Two velocity gradient tensors, denoted L_0 and L_1, produce different homogeneous steady progressive deformations that result in the same finite deformation F. That is, L_0 and L_1 are both logarithms of F. Compared to L_0, which is the principal logarithm, L_1 produces additional rotation that is undetectable in the final state at $t = 1$.

In summary, as was noted by Provost et al. (2004), the exponential function allows us to work "forward" from a velocity gradient tensor L to its resulting finite deformation tensor F, while the logarithm lets us work "backward" from F to L, in many cases uniquely.

3. Application: simultaneous deformation

Structural geologists often choose to break finite deformations into simpler components. This process of decomposition is useful because the components of a deformation are typically easier to conceptualize than the full deformation, and because field data may relate to only one of the components. Decompositions have been used to approximate the time sequence of deformation (e.g., Evans and Dunne, 1991; Mookerjee and Mitra, 2009), and to isolate specific details about strain (e.g., Bell, 1979; De Paor, 1986; Oertel and Reymer, 1992; Yonkee, 2005) or vorticity (e.g., Means et al., 1980; Lister and Williams, 1983; Jiang, 1999).

Some decompositions are accomplished through matrix multiplication (e.g., Ramsay and Huber, 1983; Means, 1994). Given two finite deformations F_1 and F_2, the matrix product $F = F_2F_1$ represents a non-steady process in which the rock is deformed first by F_1 and later by F_2. The composite deformation is called a *sequential superposition* of F_1 and F_2. The order of the factors is significant, as $F_2F_1 \neq F_1F_2$ typically. Sanderson and Marchini (1984), for example, examined how a pure shear followed by a simple shear could describe transpression and transtension. Others have used a *polar decomposition* $F = RC$ to express a finite deformation as the result of a coaxial deformation C followed by a rotation R (Malvern, 1969; Elliott, 1970; De Paor, 1983).

Another way to build complicated deformations from simpler ones is to apply the simpler deformations at the same time. This approach is termed *simultaneous superposition* of deformation. Except in special cases, the simultaneous deformation arising from F_1 and F_2 is different from the sequential deformations F_1F_2 and F_2F_1 (Tikoff and Fossen, 1993), and more difficult to compute. There are two main computational methods: split-stepping, and what we call the ln-sum-exp technique.

Split-stepping, which was introduced to structural geology by Ramberg (1975), conceptualizes simultaneous deformation as the interleaving of small increments, as follows. For any matrix F whose principal logarithm $\ln F$ is defined, one can further define the *principal nth root* of F by

$$\sqrt[n]{F} = \exp\left(\frac{1}{n}\ln F\right)$$

(see Appendix D). This $\sqrt[n]{F}$ satisfies $\left(\sqrt[n]{F}\right)^n = F$ and is termed an *increment* of the finite deformation F. Now suppose that we wish to find the simultaneous superposition F of two finite deformations F_1 and F_2. The matrix product $\left(\sqrt[n]{F_1}\sqrt[n]{F_2}\right)^n$ expresses the interleaving of increments of F_1 with increments of F_2. As n goes to infinity, the increments become finer and finer, and the interleaved matrix product approaches a limit, which is defined to be the simultaneous superposition of F_1 and F_2:

$$F = \lim_{n\to\infty}\left(\sqrt[n]{F_1}\sqrt[n]{F_2}\right)^n. \tag{3}$$

In contrast, the ln-sum-exp method works in terms of the velocity gradient tensors L_1 and L_2 corresponding to F_1 and F_2. In rock that is undergoing two simultaneous

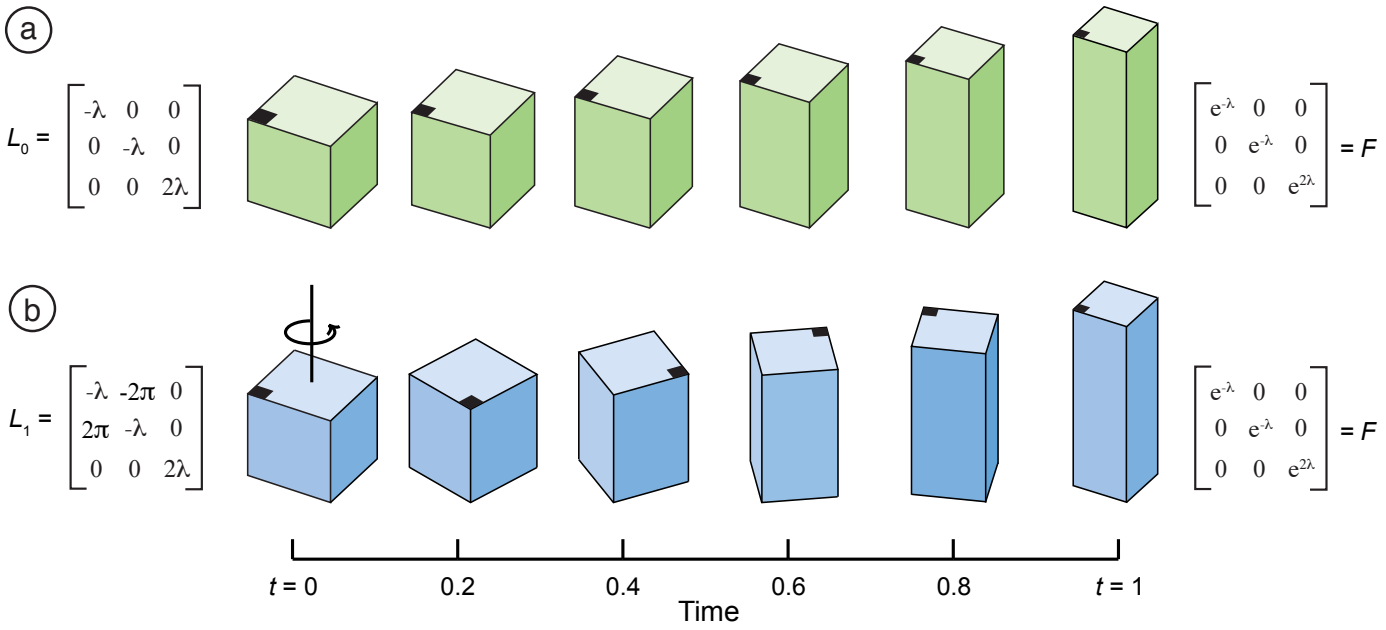

Figure 4: Two velocity gradient tensors L_0 and L_1 (from Eq. (C.1)), with $\lambda = -\ln \mu_1 = \frac{1}{2} \ln \mu_3$ for brevity and to impose volume preservation), produce distinct homogeneous steady deformation paths that result in the same finite deformation.

deformations, the combined velocity field can be taken to be the sum of the component velocity fields (Provost et al., 2004; Pollard and Fletcher, 2005, p. 178). So the velocity gradient tensor for the simultaneous deformation is $L_1 + L_2$, the path of the simultaneous deformation is

$$\vec{y} = (\exp t(L_1 + L_2))\, \vec{x},$$

and the simultaneous finite deformation tensor is $\exp(L_1 + L_2)$. Provost et al. (2004) noted that L_i can be computed from F_i as the principal logarithm $L_i = \ln F_i$. Therefore, in terms of the two finite deformation tensors F_1 and F_2, the simultaneous finite deformation tensor is

$$F = \exp(\ln F_1 + \ln F_2)\,. \tag{4}$$

Put simply, to compute the simultaneous deformation one computes two logarithms, adds them, and exponentiates — this is why we call the method "ln-sum-exp".

The Trotter product formula (see Appendix B) implies that Eqs. (3) and (4) yield the same simultaneous deformation F. Although split-stepping is useful for visualizing the process of simultaneous deformation, computing deformation tensors by Eq. (3) requires complicated algebraic argument (Ramberg, 1975), especially in three dimensions. The ln-sum-exp method is algorithmic (see Appendix F for computer code). It is therefore easier, faster, and less error-prone than split-stepping.

To provide more explicit examples of the utility of the ln-sum-exp method, we now demonstrate how to construct simultaneous transpression with triclinic symmetry in two ways.

3.1. Inclined transpression

Many natural shear zones have monoclinic symmetries, with either strike- or dip-parallel lineations. These two

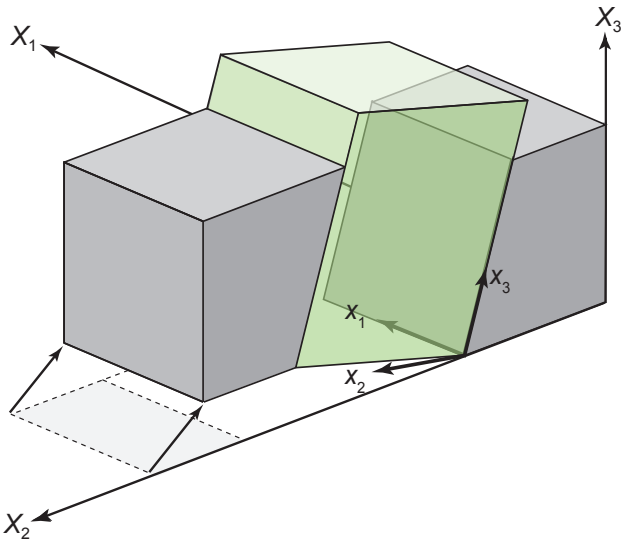

Figure 5: Diagram illustrating an inclined transpression kinematic model. The reference coordinate system $\vec{x}$ (which is different from the global coordinate system $\vec{X}$) is parallel to the shear plane. Compare with the triclinic deformation of Lin et al. (1998) from Fig. 1. Modified from Jones et al. (2004).

directions are predicted by monoclinic transpression models; whether one direction or the other develops depends on the angle of convergence across the shear zone and the amount of accumulated deformation (Fossen and Tikoff, 1993; Passchier, 1998; Teyssier and Tikoff, 1999; Ghosh, 2001; Dewey, 2002). However, some natural shear zones have oblique lineations (e.g., Hudleston et al., 1988; Goodwin and Williams, 1996; Lin et al., 1998; Czeck and Hudleston, 2004; Horsman et al., 2008), which cannot be explained by monoclinic models. Such shear zones are more realistically modeled by transpression with triclinic symmetry (Jones and Holdsworth, 1998; Lin et al., 1998; Jones et al., 2004).

Here we focus on the simultaneous inclined transpression of Jones and Holdsworth (1998) and Jones et al. (2004). This model involves two simple shear components applied to a zone that is also allowed to change its width through a coaxial deformation (Fig. 5). Written as matrices in coordinates $\vec{x}$ aligned with the shear plane, the three components of deformation are

$$\begin{bmatrix} 1 & \gamma_{xy} & 0 \\ 0 & 1 & 0 \\ 0 & 0 & 1 \end{bmatrix}, \quad \begin{bmatrix} 1 & 0 & 0 \\ 0 & 1 & 0 \\ 0 & \gamma_{zy} & 1 \end{bmatrix},$$

$$\begin{bmatrix} 1 & 0 & 0 \\ 0 & \alpha_z^{-1} & 0 \\ 0 & 0 & \alpha_z \end{bmatrix},$$

for some constants γ_{xy}, γ_{zy}, α_z. In the first step of the ln-sum-exp method, we compute the principal logarithms of these matrices to be

$$\begin{bmatrix} 0 & \gamma_{xy} & 0 \\ 0 & 0 & 0 \\ 0 & 0 & 0 \end{bmatrix}, \quad \begin{bmatrix} 0 & 0 & 0 \\ 0 & 0 & 0 \\ 0 & \gamma_{zy} & 0 \end{bmatrix},$$

$$\begin{bmatrix} 0 & 0 & 0 \\ 0 & -\ln\alpha_z & 0 \\ 0 & 0 & \ln\alpha_z \end{bmatrix}.$$

In the second step, we find the velocity gradient tensor L of the inclined transpression as the sum of these logarithms:

$$L = \begin{bmatrix} 0 & \gamma_{xy} & 0 \\ 0 & -\ln\alpha_z & 0 \\ 0 & \gamma_{zy} & \ln\alpha_z \end{bmatrix}. \tag{5}$$

For the third step, we must compute the Jordan decomposition (see Appendix A) of this combined velocity gradient tensor in order to exponentiate. Assuming that $\alpha_z \neq 1$, tL diagonalizes as

$$tL = P \begin{bmatrix} 0 & 0 & 0 \\ 0 & -t\ln\alpha_z & 0 \\ 0 & 0 & t\ln\alpha_z \end{bmatrix} P^{-1},$$

where

$$P = \begin{bmatrix} 1 & 2\gamma_{xy} & 0 \\ 0 & -2\ln\alpha_z & 0 \\ 0 & \gamma_{zy} & 1 \end{bmatrix}.$$

Therefore the progressive deformation tensor is

$$\begin{aligned} \exp tL &= P \begin{bmatrix} 0 & 0 & 0 \\ 0 & \alpha_z^{-t} & 0 \\ 0 & 0 & {\alpha_z}^t \end{bmatrix} P^{-1} \\ &= \begin{bmatrix} 1 & \gamma_{xy}\frac{1-\alpha_z^{-t}}{\ln\alpha_z} & 0 \\ 0 & \alpha_z^{-t} & 0 \\ 0 & \gamma_{zy}\frac{{\alpha_z}^t-\alpha_z^{-t}}{2\ln\alpha_z} & {\alpha_z}^t \end{bmatrix} \end{aligned}$$

and the finite deformation tensor is

$$F = \exp L = \begin{bmatrix} 1 & \gamma_{xy}\frac{1-\alpha_z^{-1}}{\ln\alpha_z} & 0 \\ 0 & \alpha_z^{-1} & 0 \\ 0 & \gamma_{zy}\frac{\alpha_z-\alpha_z^{-1}}{2\ln\alpha_z} & \alpha_z \end{bmatrix}. \tag{6}$$

The inclined transpression deformation tensor of Jones and Holdsworth (1998), which was misquoted in their later publication (Jones et al., 2004), differs from our inclined transpression tensor (6) in the F_{32} entry:

$$\begin{bmatrix} 1 & \gamma_{xy}\frac{1-\alpha_z^{-1}}{\ln\alpha_z} & 0 \\ 0 & \alpha_z^{-1} & 0 \\ 0 & \gamma_{zy}\frac{1-\alpha_z^{-1}}{\ln\alpha_z} & \alpha_z \end{bmatrix}. \tag{7}$$

Their deformation tensor (7) is incorrect. To see so, notice that the velocity gradient tensor (5) equals the velocity gradient tensor (B.1) of the triclinic transpression of Lin et al. (1998), up to these changes of notation:

$$\alpha_z = e^{\dot{\epsilon}}, \quad \gamma_{xy} = \dot{\gamma}\cos\phi, \quad \gamma_{zy} = \dot{\gamma}\sin\phi.$$

The finite deformations should be identical up to the same changes of notation. From Eq. (B.2), the finite deformation of Lin et al. (1998) is

$$\begin{bmatrix} 1 & \frac{\dot{\gamma}}{\dot{\epsilon}}(1-e^{-\dot{\epsilon}})\cos\phi & 0 \\ 0 & e^{-\dot{\epsilon}} & 0 \\ 0 & \frac{\dot{\gamma}}{\dot{\epsilon}}\sinh\dot{\epsilon}\sin\phi & e^{\dot{\epsilon}} \end{bmatrix}.$$

This matches (6), not (7).

That inclined transpression should be identical to the triclinic transpression of Lin et al. (1998) makes sense. Both describe transpression in which the shortening direction is arbitrarily oblique to the shear plane, using coordinates aligned with the shear plane. Mathematically, they differ only in the notation used to express the direction and amount of shortening. Geologically, the triclinic transpression is intended to model vertical shear planes while the inclined transpression is intended to model horizontal shortening, but this distinction is subsumed by the choice of coordinate system.

3.2. Triclinic transpression from first principles

As a second example of simultaneous deformation using the ln-sum-exp method, we now develop a new model of transpression, from first principles and in a way that illustrates the issues of boundary slip and volume preservation in kinematic models.

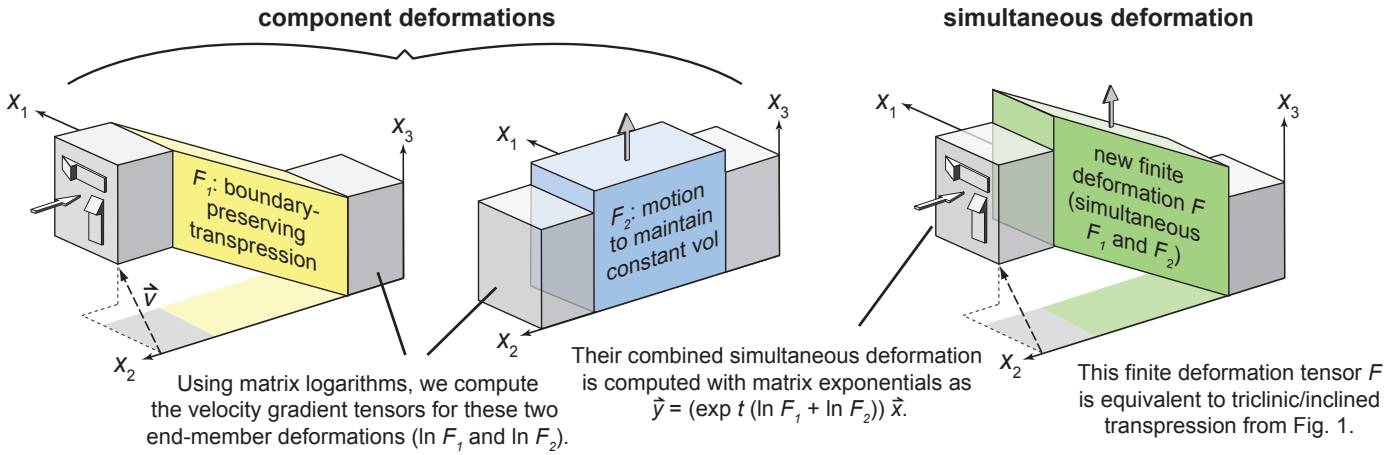

Figure 6: An example of the simultaneous combination of two component deformations. For the first component, on the left, two rigid blocks move relative to one another with arbitrary velocity $\vec{v}$; the rock between them deforms so that the boundary conditions are preserved. For the second component, in the center, the material is extruded vertically, so as to cancel the volume loss of the first deformation. The final state, solved using the ln-sum-exp method, illustrated at the right, is mathematically equivalent to triclinic and inclined transpression described in the text.

We combine the two finite deformations illustrated in Fig. 6. Material trapped between two rigid blocks is deforming ductilely as the blocks move with relative velocity $\vec{v}$. In the F_1 deformation, the deforming material is allowed to shorten (or lengthen), and shear vertically and horizontally, without any slip along the boundary planes. In coordinates aligned with the boundary planes, the deformation tensor is

$$F_1 = \begin{bmatrix} 1 & v_1 & 0 \\ 0 & 1+v_2 & 0 \\ 0 & v_3 & 1 \end{bmatrix}.$$

Unfortunately, F_1 has determinant $1+v_2$, so it does not preserve volume, except in the special case of simple shear. We can offset the volume loss (or gain) by simultaneously superimposing a dilation F_2 in the x_3-direction. Let

$$F_2 = \begin{bmatrix} 1 & 0 & 0 \\ 0 & 1 & 0 \\ 0 & 0 & \frac{1}{1+v_2} \end{bmatrix}$$

be the dilation. As in the previous example, we use the ln-sum-exp method to construct our simultaneous deformation from these two finite deformations F_1 and F_2. The velocity gradient tensor of the simultaneous deformation is

$$\begin{aligned} L &= \ln F_1 + \ln F_2 \\ &= \begin{bmatrix} 0 & \frac{v_1}{v_2}\ln(1+v_2) & 0 \\ 0 & \ln(1+v_2) & 0 \\ 0 & \frac{v_3}{v_2}\ln(1+v_2) & -\ln(1+v_2) \end{bmatrix}, \end{aligned} \tag{8}$$

and the finite deformation tensor is

$$\begin{aligned} F &= \exp L \\ &= \begin{bmatrix} 1 & v_1 & 0 \\ 0 & 1+v_2 & 0 \\ 0 & \frac{v_3}{2}\frac{2+v_2}{1+v_2} & \frac{1}{1+v_2} \end{bmatrix}. \end{aligned}$$

This tensor F is identical to F_1 in the first two rows, but not in the third. It describes a deformation in which material slips along both boundary planes in the x_3-direction. Thus, although F preserves volume it does not satisfy the boundary conditions.

It turns out that the transpression that we have just constructed is identical to the triclinic transpressions of Lin et al. (1998) and Jones and Holdsworth (1998). Again it differs only in the notation used to express the direction and amount of shortening. Specifically, the velocity gradient tensors (5) and (8) are equal up to these changes of notation:

$$\begin{aligned} \alpha_z &= (1+v_2)^{-1}, \\ \gamma_{xy} &= \frac{v_1}{v_2}\ln(1+v_2), \\ \gamma_{zy} &= \frac{v_3}{v_2}\ln(1+v_2). \end{aligned}$$

Building the transpression tensor F from the intermediate tensor F_1 emphasizes the fact that volume is preserved in transpression only by letting material slip vertically. Slip along the boundary is a valid criticism of homogeneous transpression models (Robin and Cruden, 1994). It is impossible to construct a homogeneous finite deformation, other than simple shear, that satisfies no-slip boundary conditions and preserves volume.

4. Deformation concepts and data

In this section we review a variety of deformation concepts, which are summarized graphically in Fig. 7. Loosely, the left side of the figure relates to velocity while the right side relates to position. The two sides are connected by the matrix exponential and logarithm.

For each concept, we describe the role it plays in homogeneous steady models and how it can be observed in field

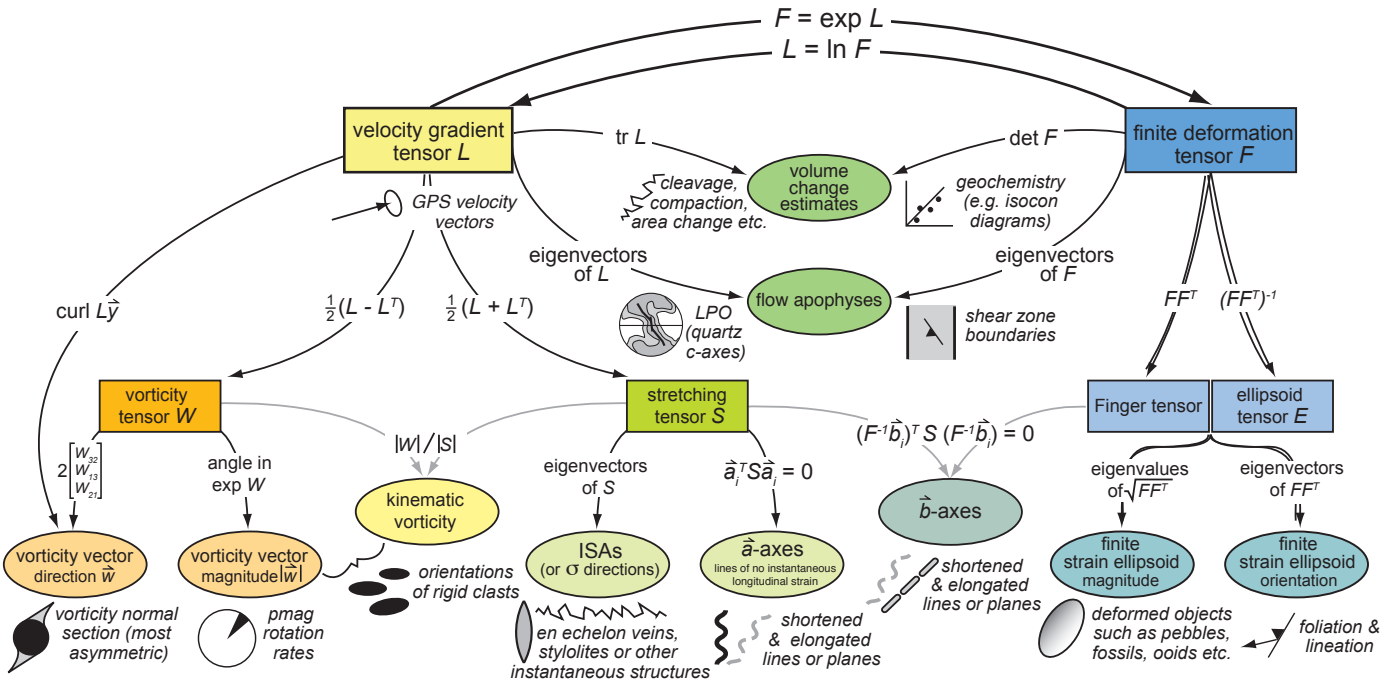

Figure 7: A summary of some of the relationships among the velocity gradient tensor L, the finite deformation tensor F, auxiliary mathematical quantities, and geological data that relate to those quantities.

data. Instead of graphical methods or formulas designed for specific kinematic models (e.g., monoclinic or triclinic transpression), we offer general, coordinate-independent mathematical facts that apply to all homogeneous steady deformations. This review is not exhaustive, but rather focuses on the concepts needed for Section 5. Most of this material is well known in the geology community. On the other hand, our equations for the $\vec{a}$- and $\vec{b}$-axes do not exist in the literature except for special cases (e.g., the L_a and L_b axes of Passchier, 1990), and our two expressions for kinematic vorticity are certainly uncommon and possibly new.

4.1. Volume change

Volume change is measured by both F and L, as is illustrated by the position of this concept in Fig. 7. The finite deformation tensor F preserves volume if and only if $\det F = 1$. Because $\det(\exp L) = \exp(\operatorname{tr} L)$, the deformation preserves volume if and only if the velocity gradient tensor has trace zero. One can also understand this by noticing that the divergence of the velocity field is $\operatorname{div} \vec{v} = \operatorname{tr} L$. In any fluid flow, divergence zero corresponds to incompressibility (e.g., Munson et al., 2009, p. 271) and therefore to volume preservation.

Volume changes are often difficult to estimate for deformed rocks. Successful estimates have been derived from geochemical methods such as isocon diagrams (Bhattacharyya and Hudleston, 2001; Baird and Hudleston, 2007), the area change of strain markers across strain gradients (Srivastava et al., 1995), and rocks with pronounced cleavage (Wright and Platt, 1982; Markley and Wojtal, 1996; Goldstein et al., 1999). It is more common, however, to assume constant volume in a deforming system in the absence of compelling evidence to the contrary.

4.2. Flow apophyses

In two-dimensional deformation, individual particles may follow hyperbolic, radiant, closed-loop, or parallel paths, depending on the geometry of flow (Ramberg, 1975; Passchier, 1997). For hyperbolic paths, the straight asymptotes to the hyperbolic paths are known as the *flow apophyses*. For simple shear, which is a degenerate case, there is only one flow apophysis, which is parallel to the particle paths. In three-dimensional deformation, particles may experience various combinations of the four path types. For example, in the deformation of Fig. 4b, particles follow spiral paths that approach the direction of elongation.

Mathematically, a flow apophysis is usually defined to be an eigenspace of the velocity gradient tensor L (Bobyarchick, 1986; Passchier, 1987a). It could just as well be defined as an eigenspace of the finite deformation tensor F (Fig. 7), because $F = \exp L$ and exponentiation preserves eigenspaces. Passchier (1997) called the flow apophysis associated to the greatest eigenvalue of L (or F) the *fabric attractor*. Material lines through the origin, that are not themselves flow apophyses, rotate toward this apophysis as time t goes to infinity. Similarly, he referred to the flow apophysis with the least eigenvalue as the *fabric repeller*, because material lines rotate away from it.

Several kinds of field data shed light on the orientation of flow apophyses: patterns of forward- and backward-

rotating clasts (Simpson and De Paor, 1993; Wallis, 1995; Jessup et al., 2007), fabric orientations relative to shear zone boundaries (Bailey and Eyster, 2003), the angle between S and C fabrics (Platt and Vissers, 1980; Platt, 1984), and the angle between mineral lattice-preferred orientations (LPO) and field foliation/lineation (e.g., Lister and Hobbs, 1980; Platt and Behrmann, 1986; Nicolas, 1989; Vissers, 1989; Wallis, 1992). However, many methods that are used to find the orientation of flow apophyses make the assumption that deformation is plane strain (Bobyarchick, 1986; Simpson and De Paor, 1993).

4.3. Finite strain ellipsoid

A homogeneous deformation F deforms a hypothetical unit sphere in the undeformed rock into an ellipsoid in the deformed rock, called the *finite strain ellipsoid*. This ellipsoid is often described using two related tensors (Fig. 7). The *Finger tensor* or *left Cauchy-Green tensor* (Malvern, 1969, p. 158, 174) is defined as $FF^\top$. The semi-axes of the ellipsoid, or *finite strain axes*, are the eigenvectors of $FF^\top$. Their lengths are the square roots of the corresponding eigenvalues of $FF^\top$. The inverse

$$\left(FF^\top\right)^{-1} = \left(F^{-1}\right)^\top \left(F^{-1}\right) \tag{9}$$

of the Finger tensor is the *ellipsoid tensor* E of Flinn (1979) and the *Cauchy tensor* c of Malvern (1969, p. 158), Means (1976, p. 198-199), and Pollard and Fletcher (2005, p. 190). The finite strain ellipsoid is the set of all points $\vec{y}$ such that $\vec{y}^\top E\vec{y} = 1$.

Many types of field data can be used to calculate the finite strain ellipsoid, such as strain markers that originally began as spheres (e.g., ooids, Cloos, 1947) or ellipsoids (e.g., pebbles, Dunnet, 1969; Elliott, 1970; Matthews et al., 1974; Lisle, 1977; Siddans, 1980a,b). Workers have also used angular changes in fossils (Nissen, 1964; Ramsay, 1967; Tan, 1973; Srivastava and Shah, 2006) and the distribution of linear makers such as veins (Sanderson, 1977; De Paor, 1981; Panozzo, 1984; Passchier, 1990; Mulchrone, 2002), to provide just a few examples.

A finite deformation F determines a unique finite strain ellipsoid $FF^\top$, but a given ellipsoid $FF^\top$ does not uniquely determine F (Flinn, 1979; Provost et al., 2004). If $F = QDR$ is the singular value decomposition of F (see Appendix A), then

$$FF^\top = QD^2Q^{-1}.$$

Given a finite strain ellipsoid $FF^\top$, one can diagonalize $FF^\top$ to obtain Q and D^2, then compute D by taking the nonnegative square roots of the diagonal elements of D^2, and therefore determine Q and D in $F = QDR$. However, the orthogonal tensor R is unknowable. In other words, if a finite deformation F produces the Finger tensor $FF^\top$, then for any orthogonal R the finite deformation FR produces the same Finger tensor, because

$$(FR)(FR)^\top = FRR^\top F^\top = FF^\top.$$

To solve for the full deformation tensor F, one must use information beyond the finite strain ellipsoid. For example, Zhang and Hynes (1995) use the orientation of a shear plane and the direction of shear to solve for F. In Section 5.1 we solve for F using the vorticity-normal section and the amount of rotation of two material lines.

4.4. Velocity gradient tensor

Until recently, geologists had few opportunities to collect data directly related to velocities and the velocity gradient tensor L. However, with the introduction of GPS, it is now possible to calculate L from modern velocity fields (e.g., Lamb, 1994a,b; Allmendinger et al., 2007, 2009). One can also recover L by combining the various other velocity-related data described throughout this section.

Two component tensors derived from L are particularly useful (Ramsay, 1967; Malvern, 1969; McKenzie, 1979). The *stretching tensor* or *rate-of-deformation tensor* $S = \frac{1}{2}\left(L + L^\top\right)$ is symmetric, and its corresponding finite deformation $\exp S$ is coaxial. The *vorticity tensor* $W = \frac{1}{2}\left(L - L^\top\right)$ is antisymmetric, and $\exp W$ is a pure rotation. The equation $L = S + W$ therefore expresses the finite deformation $F = \exp L$ as the simultaneous superposition of a coaxial deformation $\exp S$ and a rotation $\exp W$.

In some instances, the stretching and vorticity tensors themselves are used for geologic applications. For example, these tensors are calculated from GPS velocity fields by Allmendinger et al. (2007) to predict regions of distortion and rotation in a variety of tectonic environments for comparison with long-lived geologic features. More commonly geologic field data determine secondary mathematical quantities related to S and W, which we discuss in the remainder of this section.

4.5. Instantaneous stretching axes

In two dimensions, the *instantaneous stretching axes* (ISAs) are the directions of maximum and minimum longitudinal strain rate — that is, the material lines that are elongating and shortening most rapidly (Ramsay, 1967; Means et al., 1980; Lister and Williams, 1983). Mathematically, they are the eigenvectors of the stretching tensor S. In three dimensions, a third eigenvector of S and hence a third ISA occurs, with some intermediate longitudinal strain rate. The ISAs are always perpendicular to each other.

It is worth emphasizing that the ISAs are constant in any homogeneous steady deformation as defined by Eq. (1). Therefore *spin*, which is the rotation of the ISAs as deformation progresses (Lister and Williams, 1983), cannot occur. For an example of spin in non-steady models, see Jiang (1994).

Structures that record only a small amount of deformation, such as *en echelon* veins, stylolites, dikes, borehole breakouts, and faults, are often interpreted to reflect paleostress or modern stress directions (e.g., Zoback and

Zoback, 1980; Pollard et al., 1982; Zoback et al., 1985; Gudmundsson, 1990; Anglier, 1994; Nemcock and Lisle, 1995; Petit and Mattauer, 1995; Koehn et al., 2007). In some cases, these types of data may be more correctly interpreted as reflecting the ISAs (e.g., Twiss and Unruh, 1998).

4.6. Lines of zero instantaneous longitudinal strain

At any instant, the deforming rock contains lines of zero instantaneous longitudinal strain (Ramsay, 1967, p. 173), meaning lines that are neither elongating nor shortening. Mathematically, these lines consist of all points $\vec{y}$ that satisfy $\vec{y}^{\top} S \vec{y} = 0$. In three-dimensional space, the lines are not isolated, but rather trace out a cone, which we call the $\vec{a}$*-cone* (Fig. 8). This cone separates regions of instantaneous shortening and elongation. Eigenvectors of S, whose associated eigenvalues are negative, lie in the shortening region, while eigenvectors with positive eigenvalues lie in the elongating region. If the deformation is plane strain, then the cone degenerates into a pair of planes that intersect along the eigenvector of S with eigenvalue 0.

On any planar cross-section of three-dimensional space through the origin, the $\vec{a}$-cone appears as a pair of lines (Fig. 8). Working in the context of plane strain, Passchier (1990) called these lines *L-axes*, and denoted them La_1 and La_2 when thinking of them as material lines. We instead call these lines $\vec{a}$*-axes*, and denote them as vectors $\vec{a}_1$ and $\vec{a}_2$ (see Fig. 7), to avoid confusion with the velocity gradient tensor L.

A material line that begins the deformation lying in (along) the $\vec{a}$-cone may or may not remain in the cone. The deformation may rotate the material line into either the shortening or elongating region. If we regard the entire $\vec{a}$-cone as a cone of material, then we can consider where the finite deformation F moves this cone. In fact, F will move the cone to some other cone, which we call the $\vec{b}$*-cone*, consisting of all points $\vec{y}$ such that $\left(F^{-1}\vec{y}\right)^{\top} S \left(F^{-1}\vec{y}\right) = 0$. Like the $\vec{a}$-cone, the $\vec{b}$-cone intersects any plane through the origin as a pair of lines (Fig. 8). We call these the $\vec{b}$*-axes* and denote them $\vec{b}_1$ and $\vec{b}_2$ (instead of the Lb_1 and Lb_2 of Passchier (1990)). We note that the $\vec{a}$-cone and $\vec{b}$-cone are both different from the lines (surface) of zero *finite* longitudinal strain described by Ramsay (1967, p. 66) and Talbot (1970).

As illustrated by their position within Fig. 7, the $\vec{b}$-axes cannot be computed strictly from S, but require knowledge of F as well. In plane-strain deformation, one may infer that material lines originally oriented along the $\vec{a}_i$ are sent to the $\vec{b}_i$ by the deformation — that is, $F\vec{a}_1$ and $F\vec{a}_2$ are parallel to $\vec{b}_1$ and $\vec{b}_2$. For non-plane-strain deformation, however, this assumption does not hold. Instead, lines on the $\vec{a}$-axis cone move to lines on the $\vec{b}$-axis cone, without being confined to any particular plane such as the vorticity-normal section.

Assuming that the deformation is not too large, all material lines will experience either shortening-then-

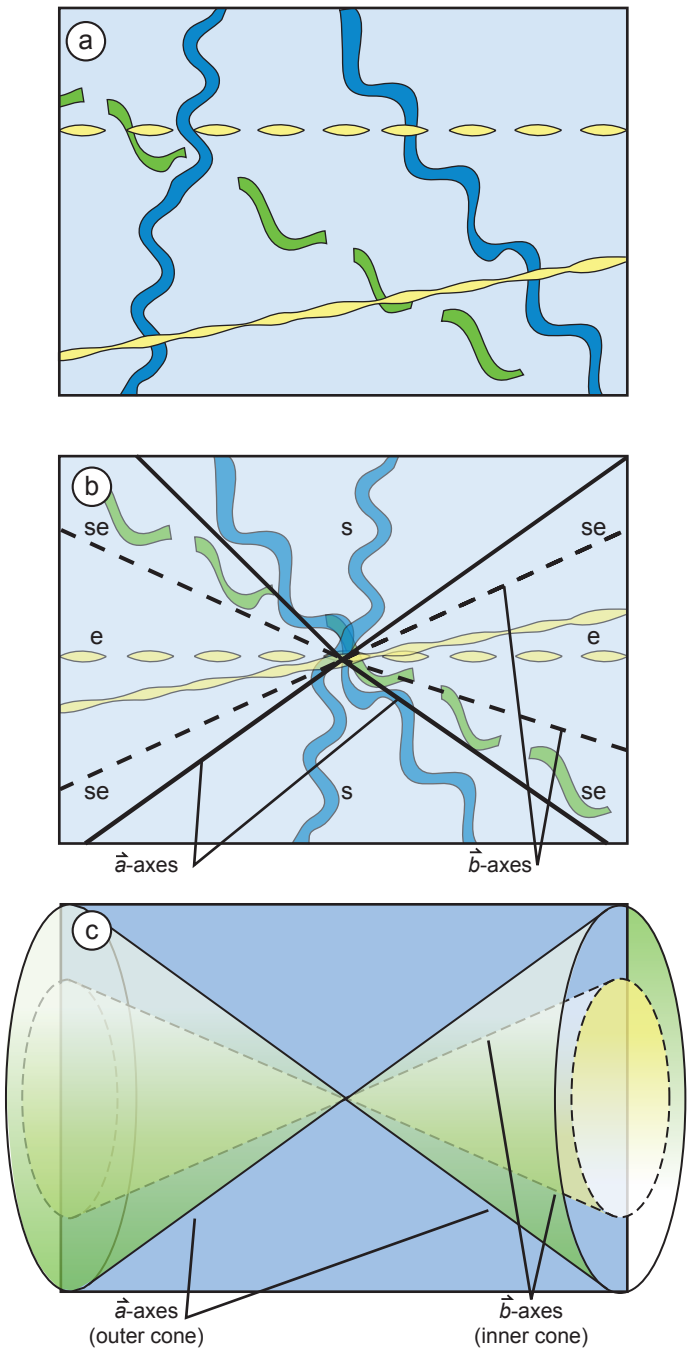

Figure 8: (a) A cartoon for the types of vein behaviors that might be observed on a plane, including veins that have only shortened (blue), those that have only elongated (yellow), and those that have experienced shortening then elongation (green). (b) The orientations of these veins are used to define the $\vec{a}$-axes, which separate regions of shortening (s) from regions of elongation (e and se), and the $\vec{b}$-axes, which separate the regions of elongation-only (e) from those that have experienced shortening followed by elongation (se). (c) In three dimensions there are $\vec{a}$-cones (green) and $\vec{b}$-cones (yellow), that intersect the observation plane in the $\vec{a}$- and $\vec{b}$-axes from (b).

elongation, elongation-then-shortening, shortening only, or elongation only (Talbot, 1970; Passchier, 1990). Typically the $\vec{b}$-axes separate the elongation-only region from the shortening-then-elongation region, and the $\vec{a}$-axes separate the shortening-only region from the shortening-then-elongation region (Fig. 8). (A more detailed characterization of the possible configurations of $\vec{a}$- and $\vec{b}$-axes is beyond the scope of this paper, but see Appendix F for an example of elongating-shortening-elongating behavior.) Field data such as folded and boudinaged veins have been used to constrain the $\vec{a}$- and $\vec{b}$-cones in several studies (e.g., Passchier and Urai, 1988; Wallis, 1992; Kumerics et al., 2005; Short and Johnson, 2006).

4.7. Vorticity vector

The *vorticity vector* $\vec{w}$ of a progressive deformation is defined to be the curl of the velocity vector field $\dot{\vec{y}}$ (Malvern, 1969; Means et al., 1980; Xypolias, 2010):

$$\vec{w} = \operatorname{curl}(\dot{\vec{y}}) = \begin{bmatrix} L_{32} - L_{23} \\ L_{13} - L_{31} \\ L_{21} - L_{12} \end{bmatrix} = 2 \begin{bmatrix} W_{32} \\ W_{13} \\ W_{21} \end{bmatrix}.$$

Notice that $\vec{w}$ depends on only L — not on $\vec{y}$, $\vec{x}$, or t — for a flow that is homogeneous and steady.

The plane perpendicular to the vorticity vector, termed the *vorticity-profile plane* (Robin and Cruden, 1994) or the *vorticity-normal section* (Jiang and Williams, 1998), can often be diagnosed in the field as the plane with the most asymmetric features. This face is important to determine since it yields information on the sense of shear in movement zones (Lister and Williams, 1979). Many workers implicitly assume that the vorticity vector is normal to the X-Z-plane of the finite strain ellipsoid, which is required by many vorticity analysis methods (Simpson and De Paor, 1997; Law et al., 2004; Jessup et al., 2007). However, this assumption does not hold for all deformations. In cases where triclinic symmetry is inferred from field data (e.g., Czeck and Hudleston, 2003), it is critical to examine faces other than the three principal strain sections, to characterize the orientation of the vorticity vector accurately. In Section 5.2 we show that assuming a particular orientation for the vorticity vector can have dramatic effects on model results.

4.8. Vorticity scalar

The *vorticity (scalar)* w is defined as the length of the vorticity vector:

$$w = |\vec{w}| = 2\sqrt{{W_{32}}^2 + {W_{13}}^2 + {W_{21}}^2}.$$

The eigenvalues of W are 0 and $\pm\frac{1}{2}wi$. The finite deformation $\exp W$ rotates material $\frac{1}{2}w$ radians about the eigenvector of W with eigenvalue 0. (In the two-dimensional case, the eigenvalues are just $\pm\frac{1}{2}wi$, and $\exp W$ rotates about the origin.)

Information about the amount of rigid rotation in a deforming body, and hence about w, can be obtained from paleomagnetic data such as vertical axis rotations (McKenzie and Jackson, 1983).

4.9. Kinematic vorticity

The *kinematic vorticity* W_k (Truesdell, 1953; Means et al., 1980) of a progressive deformation is a measure of the relative amounts of vorticity and stretching. It can be defined as

$$W_k = \frac{|W|}{|S|},$$

where, for any matrix A, $|A|$ denotes the square root of the sum of the squares of the entries of A (see Appendix E). In one extreme case, when $L = S$ and $W = 0$, the deformation has $W_k = 0$ and is purely distortional. At the other extreme, when $L = W$ and $S = 0$, the deformation has infinite W_k and is purely rotational.

The kinematic vorticity is also related to the eigenvalues $\lambda_1, \lambda_2, \lambda_3$ of L by

$$W_k = \sqrt{1 - \frac{{\lambda_1}^2 + {\lambda_2}^2 + {\lambda_3}^2}{|S|^2}}$$

(see Appendix E). If L has only real eigenvalues, then ${\lambda_1}^2 + {\lambda_2}^2 + {\lambda_3}^2 \geq 0$ and so $W_k \leq 1$. This real-eigenvalue case encompasses all of the classic kinematic models (e.g., pure shear, simple shear) and all deformations expressible in the framework of Tikoff and Fossen (1993). This expression for W_k also implies that any L with $W_k > 1$ must have non-real eigenvalues. Non-real eigenvalues introduce a rotational character to the progressive deformation, which explains the periodic, "pulsating" phenomena noted by various authors (Ramberg, 1975; Means et al., 1980).

It merits emphasizing that W_k, being a single number, cannot completely characterize a homogeneous steady deformation (Tikoff and Fossen, 1995). Consider, for any $\lambda \neq 0$ and integer k, the tensor

$$L = \begin{bmatrix} -\lambda & -2k\pi & 0 \\ 2k\pi & -\lambda & 0 \\ 0 & 0 & 2\lambda \end{bmatrix}.$$

(This is the volume-preserving case of Eq. (C.1); see Fig. 4.) The eigenvalues are 2λ and $-\lambda \pm k2\pi i$. The kinematic vorticity is

$$W_k = \frac{2\pi}{\sqrt{3}} \left| \frac{k}{\lambda} \right|,$$

which can be made arbitrarily small or large by adjusting λ and k. It follows that simple shear is not the only deformation with $W_k = 1$, and that an L with $W_k \leq 1$ can have non-real eigenvalues.

Kinematic vorticity values are computed from field data using a variety of techniques (e.g., Xypolias, 2010). Some

techniques rely on rigid clasts (Jeffery, 1922; Ghosh and Ramberg, 1976; Giorgis and Tikoff, 2004) or, on larger scale, rigid crustal blocks (Giorgis et al., 2004). Many methods are graphical, where users plot the relationship between clast orientation and aspect ratio on specialized diagrams (Passchier, 1987b; Simpson and De Paor, 1993; Wallis, 1995; Simpson and De Paor, 1997; Jessup et al., 2007). Care should be taken in the field, however, because kinematic vorticity may be highly sensitive to one's choice of a vorticity vector. This point is discussed further in Section 5.2, Fernández and Díaz-Azpiroz (2009), and Xypolias (2010).

5. Application: best-fit models of field data

For our second major application of matrix exponentials and logarithms, we reanalyze a small dataset from Wallis (1992), a classic paper in the kinematic vorticity literature. We describe two models, of differing sophistication, that both integrate position and velocity data in the spirit of Fig. 7.

Wallis (1992) studied deformed metacherts in the Sanbagawa belt in Japan (Fig. 9). His data included (a) orientations of deformed veins (shortened only, shortened-then-elongated, and elongated only), (b) one measurement of the finite strain ellipsoid from thin sections through principal planes, and (c) a quartz LPO from one thin section.

Using the relationships outlined in the previous section, we express the Wallis (1992) data mathematically, in coordinates aligned with the X-, Y-, and Z-axes of the observed finite strain ellipsoid. Based on shortening and elongation patterns of veins (Fig. 9a), $\vec{a}_1$ is at 32° to 40°, $\vec{a}_2$ is at 120° to 127°, $\vec{b}_1$ is at 12° to 20°, and $\vec{b}_2$ is at 155° to 169° (measured counterclockwise from the X-axis in the X-Z-plane). Based on the finite strain ellipsoid measurements (Fig. 9b), the Finger tensor is

$$FF^\top = \begin{bmatrix} {\mu_1}^2 & 0 & 0 \\ 0 & {\mu_2}^2 & 0 \\ 0 & 0 & {\mu_3}^2 \end{bmatrix}, \tag{10}$$

where μ_1/μ_3 is between 3.4 and 3.6 and μ_2/μ_3 is between 1.6 and 1.7.

Wallis (1992) used the quartz LPO pattern to determine the orientation of a flow apophysis, by comparing the orientation of foliation (east-west and vertical) to the normal to the skeleton pattern as it passes through the center of the lower hemisphere projection (Fig. 9c). These data were collected in the X-Z-plane, and their interpretation essentially assumes plane-strain conditions. Thus the vorticity vector $\vec{w}$ is perpendicular to the X-Z-plane, the lines $\vec{a}_i$ are sent to the lines $\vec{b}_i$ by the deformation, and the flow apophysis lies in the plane at 5° to 8° (measured from the X-axis). Wallis justified his plane-strain assumption by noting that the finite strain ellipsoid plots close to plane strain on the Flinn diagram (Fig. 9b).

Wallis (1992) analyzed these data in two ways, with a goal of estimating the mean kinematic vorticity W_m. Both approaches rely on a Mohr circle method (Passchier, 1990), but the first approach uses only the vein deformation patterns ($\vec{a}$- and $\vec{b}$-axes), while the second uses only the finite strain ellipsoid and LPO. Wallis found $0.51 < W_m < 0.7$ from his first estimate and $0.35 < W_m < 0.6$ from his second. Because $0 < W_m < 1$, Wallis concluded that the deformation included simple shear ($W_m = 1$) and pure shear ($W_m = 0$) components, and not solely simple shear, as was suggested by a previous worker (Faure, 1985).

Wallis' preferred measure of kinematic vorticity, W_m, is based on the *neutral* (Passchier, 1988a) or *sectional* (Passchier, 1997) kinematic vorticity number W_n, which is different from W_k. To our knowledge, W_n has been defined only for deformations in which the vorticity vector is parallel to an ISA (Xypolias, 2010). Because we do not restrict ourselves to such deformations, we work with W_k instead of W_m. As we show below, the uncertainty in kinematic vorticity is large enough that the distinction between W_m and W_k is not important.

5.1. First model

Our first attempt at modeling is non-rigorous in two aspects. First, like Wallis (1992), this model relies on a significant assumption related to plane strain. Second, the model prioritizes some of the data (the Finger tensor) over others (the $\vec{a}$- and $\vec{b}$-axes) for no particular reason. We include this first model in our exposition because it demonstrates that our techniques can produce results similar to Wallis', it provides a real example of recovering the velocity gradient tensor from the finite deformation tensor, and it is simpler than our second model.

The basic approach is as follows. Using the Finger tensor data, we recover the finite deformation F up to a rotational ambiguity (see Section 4.3). We resolve the ambiguity using the $\vec{a}$- and $\vec{b}$-axes and a plane-strain-like assumption. Knowing F completely, we then compute L and other quantities, to check the quality of the model. For clarity of exposition we work an example based on the mean values for the data and an assumption of volume preservation. After the example, we account for variation in the data and the possibility of volume change.

In our example, the Finger tensor (10) is

$$FF^\top = \begin{bmatrix} 3.80 & 0 & 0 \\ 0 & 0.84 & 0 \\ 0 & 0 & 0.31 \end{bmatrix}. \tag{11}$$

Using the technique described in Section 4.3 we deduce the singular value decomposition $F = QDR$ from $FF^\top$. Wallis' Finger tensor is already diagonal (because we are working in coordinates aligned with the finite strain ellipsoid), so $Q = I$ is trivial and

$$D = QD = \sqrt{FF^\top} = \begin{bmatrix} 1.95 & 0 & 0 \\ 0 & 0.92 & 0 \\ 0 & 0 & 0.56 \end{bmatrix}.$$

As discussed in Section 4.3, we must use additional data to determine the rotation R such that $F = QDR$.

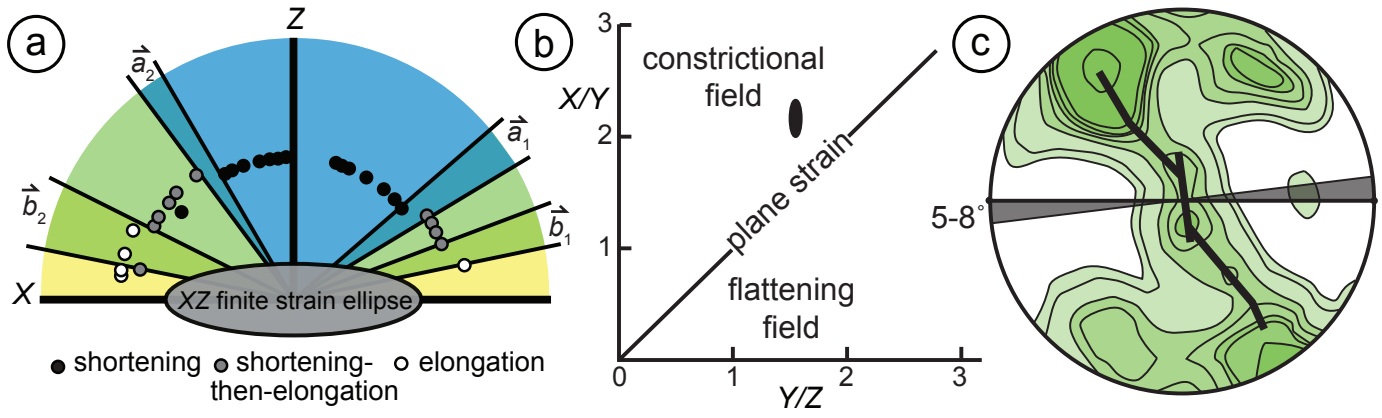

Figure 9: The three kinds of data from Wallis (1992) used to estimate a range of values for mean kinematic vorticity. (a) Vein behavior measured on thin sections parallel to the X-Z strain face. (b) The finite strain ellipsoid is estimated by finding the aspect ratio of deformed radiolarians on the X-Y-, Y-Z-, and X-Z-planes and assuming no volume change. (c) Quartz c-axes orientations measured from one thin section. Data are plotted such that foliation is EW-striking and vertical and lineation is EW-trending and horizontal. The skeleton pattern through the contoured c-axes is shown in bold; the normal to this skeleton is drawn through the center of the diagram to find the angular difference between the flow apophysis and the foliation demonstrating that deformation was sinistral for these rocks.

If the deformation were plane strain, then two material lines, that were initially parallel to the $\vec{a}$-axes, would be moved to final positions that were parallel to the $\vec{b}$-axes. In this first model, let us assume so. That is, assume that $\vec{b}_i$ is parallel to $F\vec{a}_i = QDR\vec{a}_i$. Therefore $(QD)^{-1}\vec{b}_i$ is parallel to $R\vec{a}_i$. The data tell us that $\vec{b}_1$ and $\vec{b}_2$ are oriented at 16° and 162°. We compute that $(QD)^{-1}\vec{b}_1$ and $(QD)^{-1}\vec{b}_2$ are oriented at 45.1° and 131.4°, whereas $\vec{a}_1$ and $\vec{a}_2$ are oriented at 36° and 124°. Averaging the differences in angles, we conclude that a counterclockwise rotation of the X-Z-plane through 8.2° is needed to take $\vec{a}_i$ to $(QD)^{-1}\vec{b}_i$. Thus

$$R = \begin{bmatrix} \cos 8.2^\circ & 0 & -\sin 8.2^\circ \\ 0 & 1 & 0 \\ \sin 8.2^\circ & 0 & \cos 8.2^\circ \end{bmatrix}.$$

It follows that

$$F = QDR = \begin{bmatrix} 1.93 & 0 & -0.28 \\ 0 & 0.92 & 0 \\ 0.08 & 0 & 0.55 \end{bmatrix}.$$

Now that we have modeled the finite deformation F, let us test how well the model predicts the other data from Wallis (1992) that were not used in its construction. Because F has distinct positive eigenvalues, it has a unique real logarithm

$$L = \ln F = \begin{bmatrix} 0.66 & 0 & -0.25 \\ 0 & -0.08 & 0 \\ 0.07 & 0 & -0.58 \end{bmatrix}.$$

The flow apophyses are the eigenvectors of L or F (Section 4.2). The model predicts an apophysis in the X-Z-plane oriented at 3°; this is less than, but compatible with, the 5°–8° range from the LPO data. Solving $\vec{x}^\top S\vec{x} = 0$ yields the lines of zero longitudinal strain rate. The model predicts that they lie at 43° and 129°, which are greater than, but compatible with, the angle ranges for $\vec{a}_1$ and $\vec{a}_2$ from the vein orientation data. The model predicts a kinematic vorticity of $W_k = |W|/|S| = 0.26$.

In this example, we have used mean values for all of Wallis' data and we have assumed volume preservation ($\det F = 1$). To account for uncertainty in the original data, we repeat the modeling process many times, letting μ_1/μ_3, μ_2/μ_3, $\vec{a}_1$, $\vec{a}_2$, $\vec{b}_1$, and $\vec{b}_2$ vary over their full ranges. Additionally we consider models in which $\det F$ varies between 0.9 and 1.1. The results are summarized in Table 1. They demonstrate that we recover the range of values observed in the original field data and the range of results from Wallis (1992).

5.2. Second model

Our second modeling attempt is more rigorous than the first. We make no plane-strain assumptions, and we treat all of the data symmetrically instead of prioritizing some data over others. The basic idea is to restate the data of Wallis (1992) as equations in an unknown velocity gradient tensor L and solve the equations in a least-squares sense. Then, we compute F and other quantities to check the model. We demonstrate best-fit models for seven different forms of L, from the most restricted (simple shear) to the most general (arbitrary real L).

As many as nine degrees of freedom exist when choosing L, so we require nine equations to determine L uniquely. First, the Finger tensor produced by L must match the finite strain ellipsoid data, which yields the equation

$$(\exp L)(\exp L)^\top = FF^\top,$$

where the left-hand side (LHS) is unknown and the right-hand side (RHS) is known from Eq. (11). This is an equation of symmetric 3×3 matrices, and hence amounts to six scalar equations. Next, the two lines $\vec{a}_i$ give two equations

$$\vec{a}_i^\top \frac{1}{2}\left(L + L^\top\right)\vec{a}_i = 0,$$

	Wallis' range	modeled range	modeled mean
apophysis	5°–8°	−2°–11°	4°
$\vec{a}_1$	32°–40°	33°–51°	42°
$\vec{a}_2$	120°–127°	120°–138°	129°
W_m or W_k	0.35–0.70	0.00–0.71	0.29

Table 1: Comparison of data and results from Wallis (1992) and the values predicted by our first modeling approach. The data that were used to construct the model are described in the text.

where the $\vec{a}_i$ are known. Similarly, the two lines $\vec{b}_i$ give two equations, because $F^{-1}\vec{b}_i$, which equals $(\exp -L)\vec{b}_i$, must be a line of zero longitudinal strain rate:

$$\vec{b}_i^{\top}(\exp -L)^{\top}\frac{1}{2}(L+L^{\top})(\exp -L)\vec{b}_i = 0.$$

Thus we have ten equations to determine the nine unknowns in L.

No exact solution to the ten equations can be expected, but we can find the L closest to a solution, and hence the best-fit homogeneous steady deformation, using nonlinear least squares. Namely, if the ith equation is $\mathrm{LHS}_i = \mathrm{RHS}_i$, then let

$$f(L) = \sum_{i=1}^{10} \left(\mathrm{LHS}_i - \mathrm{RHS}_i\right)^2.$$

Then f is nonnegative and $f = 0$ exactly at the solutions of the equations. We numerically minimize f to find the L that comes closest to a solution.

The preceding description is sufficient for fitting arbitrary real L. To restrict the best-fit process to X-Z-plane-strain models (the kind considered by Wallis (1992)), we set $L_{12} = L_{21} = L_{23} = L_{32} = 0$ before finding the best fit for the other parameters. To restrict the best-fit process to real-eigenvalue L, it is computationally convenient to work with the rotational Schur decomposition (see Appendix A) of L rather than L itself. That is, we substitute $L = QUQ^{\top}$ into the ten equations, where U is upper-triangular and Q is a rotation. Of L's nine degrees of freedom, three are in Q. For example, Q can be expressed as a product of rotations about the coordinate axes, such as

$$\begin{aligned} Q \;=\; & \begin{bmatrix} \cos\theta_3 & -\sin\theta_3 & 0 \\ \sin\theta_3 & \cos\theta_3 & 0 \\ 0 & 0 & 1 \end{bmatrix} \\ & \cdot \begin{bmatrix} \cos\theta_2 & 0 & \sin\theta_2 \\ 0 & 1 & 0 \\ -\sin\theta_2 & 0 & \cos\theta_2 \end{bmatrix} \\ & \cdot \begin{bmatrix} 1 & 0 & 0 \\ 0 & \cos\theta_1 & -\sin\theta_1 \\ 0 & \sin\theta_1 & \cos\theta_1 \end{bmatrix}, \end{aligned}$$

or as the exponential of an antisymmetric matrix:

$$Q = \exp \begin{bmatrix} 0 & -\theta_3 & \theta_2 \\ \theta_3 & 0 & -\theta_1 \\ -\theta_2 & \theta_1 & 0 \end{bmatrix}.$$

(These two Qs are sequential and simultaneous rotation about the coordinate axes, respectively.) The other six of L's degrees of freedom are in

$$U = \begin{bmatrix} U_{11} & U_{12} & U_{13} \\ 0 & U_{22} & U_{23} \\ 0 & 0 & U_{33} \end{bmatrix}.$$

To find an arbitrary real-eigenvalue L, we use this U as it is. To restrict the class of model further, we set certain entries of U to specific values. For example, the triclinic transpression velocity gradient tensor of Eq. (B.1) is made upper-triangular by

$$\begin{bmatrix} 0 & \dot\gamma\cos\phi & 0 \\ 0 & -\dot\epsilon & 0 \\ 0 & \dot\gamma\sin\phi & \dot\epsilon \end{bmatrix} = T \begin{bmatrix} 0 & 0 & \dot\gamma\cos\phi \\ 0 & \dot\epsilon & \dot\gamma\sin\phi \\ 0 & 0 & -\dot\epsilon \end{bmatrix} T^{\top},$$

where

$$T = \begin{bmatrix} 1 & 0 & 0 \\ 0 & 0 & 1 \\ 0 & 1 & 0 \end{bmatrix}.$$

Therefore we can find the best-fit triclinic transpression using U of the form

$$U = \begin{bmatrix} 0 & 0 & U_{13} \\ 0 & U_{22} & U_{23} \\ 0 & 0 & -U_{22} \end{bmatrix}.$$

Table 2 presents the results of our modeling using average values for the data of Wallis (1992). We found the best-fit model in seven model classes of increasing sophistication: simple shear, plane strain in the X-Z-plane, monoclinic transpression, triclinic transpression, triclinic transpression with inclined extrusion, general deformation with real-eigenvalue L, and general deformation (i.e. arbitrary real L). All of the models are presented in global coordinates (those aligned with the finite strain ellipsoid), so that they may be directly compared to each other. Because most of the models were computed via the rotational Schur decomposition, we can also present them in local coordinates that display the symmetries of each model more clearly than do global coordinates. However, the local coordinate systems vary from model to model, so the local forms of the tensors cannot be directly compared.

What is striking about the modeling results is the variation in kinematic vorticity. Plane strain in the X-Z-plane, which is essentially the model class used by Wallis (1992), produces $W_k = 0.39$. As more degrees of freedom are incorporated into the modeling, W_k steadily climbs from this

	DF	W_k	F (local coordinates)	F (global coordinates)
simple shear	4	1	$\begin{bmatrix} 1 & 1.38 & 0 \\ 0 & 1 & 0 \\ 0 & 0 & 1 \end{bmatrix}$	$\begin{bmatrix} 1.54 & -0.67 & 0.89 \\ 0.14 & 0.82 & 0.24 \\ -0.22 & 0.27 & 0.64 \end{bmatrix}$
X-Z-plane strain	5	0.39		$\begin{bmatrix} 1.83 & 0 & -0.47 \\ 0 & 0.92 & 0 \\ 0.05 & 0 & 0.56 \end{bmatrix}$
monoclinic transpression	5	0.40	$\begin{bmatrix} 1 & 0.69 & 0 \\ 0 & 1.78 & 0 \\ 0 & 0 & 0.56 \end{bmatrix}$	$\begin{bmatrix} 1.89 & -0.46 & -0.09 \\ 0.22 & 0.88 & 0.03 \\ -0.01 & 0.05 & 0.57 \end{bmatrix}$
triclinic/inclined transpression	6	0.47	$\begin{bmatrix} 1 & 0.66 & 0 \\ 0 & 1.75 & 0 \\ 0 & -0.36 & 0.57 \end{bmatrix}$	$\begin{bmatrix} 1.86 & -0.42 & -0.38 \\ 0.20 & 0.90 & 0.00 \\ 0.04 & 0.00 & 0.56 \end{bmatrix}$
triclinic transpression with inclined extrusion	8	0.66	$\begin{bmatrix} 0.58 & -0.26 & 0 \\ 0 & 1.25 & 0 \\ 0 & 1.03 & 1.39 \end{bmatrix}$	$\begin{bmatrix} 1.79 & -0.65 & -0.39 \\ 0.32 & 0.86 & 0.04 \\ 0.04 & -0.03 & 0.56 \end{bmatrix}$
L with real eigenvalues	9	1.00	$\begin{bmatrix} 1.00 & -0.76 & 0.59 \\ 0 & 1.00 & -1.02 \\ 0 & 0 & 1.00 \end{bmatrix}$	$\begin{bmatrix} 1.71 & 0.78 & -0.51 \\ -0.43 & 0.76 & -0.29 \\ 0.00 & 0.18 & 0.53 \end{bmatrix}$
general L	9	2.95		$\begin{bmatrix} 0.57 & 0.92 & -1.61 \\ -0.51 & -0.56 & -0.51 \\ -0.43 & 0.35 & 0.05 \end{bmatrix}$

Table 2: Results from our second method of modeling data from Wallis (1992). Columns include the number of degrees of freedom (DF), the kinematic vorticity (W_k), and the finite deformation tensor in global and local (where appropriate) coordinate systems. Numbers with decimal points were computed during the best-fit process; numbers without decimal points were fixed before the best-fit process.

value. It reaches 1.00 in the sixth model, which is the best fit among all models with real-eigenvalue velocity gradient tensors L. Coincidentally, $W_k = 1.00$ is consistent with the simple shear interpretation of Faure (1985), which Wallis (1992) set out to refute.

The sixth model has only one independent eigenvector, and its kinematic vorticity is the largest that can be achieved with real eigenvalues. These facts suggest that the real-eigenvalue condition significantly constrains the best-fit process, which is worrisome because geology does not require L to have real eigenvalues (e.g., Iacopini et al., 2010). The final row of the table shows the result of allowing L with arbitrary complex eigenvalues: The kinematic vorticity increases to 2.95. This result suggests that to match the available data the deformation must have a large rotational component.

6. Discussion and conclusion

Matrix exponentials are not new. They were defined by Laguerre in 1867 and applied to differential equations as early as 1938 (Higham, 2008). The matrix exponential solution of Eq. (1) is fundamentally equivalent to any other method of solving this simple differential equation. Nevertheless the exponential/logarithm framework is valuable to the analysis of geological deformation in several ways.

First, Eq. (1) and Eq. (2) are not tied to any particular coordinate system or model subclass. They express all homogeneous steady models, from the simple shear of Ramsay and Graham (1970) to the general deformation of Soto (1997), in a single closed-form expression that can be computed algorithmically, either numerically or symbolically. The matrix exponential simplifies the mathematical presentation of homogeneous steady deformations and clarifies the relationships among concepts. For example, the velocity gradient tensor L and finite deformation tensor F have the same eigenspaces (the flow apophyses). This fact can be deduced in several different ways, but the exponential yields a particularly simple proof. In Section 5, the exponential lets us convert both velocity- and position-related data into explicit equations to be fit by a model. Because so many kinds of data are made available to the fitting process, we can try models with many degrees of freedom and explore how different classes of models affect our conclusions.

Second, without the exponential we would be unlikely to stumble upon the logarithm, which is concretely useful. For example, computing algebraic expressions of simultaneous deformations by the ln-sum-exp method is dramatically easier than computing them by split-stepping. Also, the logarithm lets us interpolate finite deformations by progressive deformations, yielding a helpful visualization tool (see Appendix F).

Third, although this review article has focused on providing a complete description of all homogeneous steady deformations, our framework can also be applied to geologically more-realistic non-steady deformations. For example, Provost et al. (2004) extended Eq. (2) to some special

non-steady cases (see Appendix B). Steady deformations can also be sequenced to model a non-steady deformation (Section 3). The theory of steady deformations can be used negatively, to show that a given dataset could not have arisen through a steady process (e.g., Horsman and Tikoff, 2007). Also, to solve a non-steady differential equation, one typically resorts to numerical approximation methods such as the Euler method, each step of which is steady and hence treatable by our framework (see Section 6.1 below).

Finally, the exponential framework reveals a hidden mathematical structure underlying rock deformation. The set of all homogeneous finite deformations forms a *Lie group* — a set of transformations or symmetries (see, e.g., Belinfante and Kolman, 1972; Gilmore, 1974; Curtis, 1984; Hall, 2003; Pollatsek, 2009). The Lie group of homogeneous finite deformations is profitably viewed as a curved subset of the set of all 3×3 matrices. Meanwhile, the set of all velocity gradient tensors forms a related structure, which mathematicians call the *Lie algebra* associated to the Lie group. The Lie algebra is a flat vector space. The matrix exponential function "wraps" the flat Lie algebra around the curved Lie group in a well-behaved way (Fig. 10a). In many cases, questions about a Lie group can be recast as easier questions about its Lie algebra (Gilmore, 1974, p. 117). The ln-sum-exp technique of Section 3 is an example: To simultaneously superimpose two homogeneous deformations, we "pull them back" to the Lie algebra using the matrix logarithm, add them there, and then "push" the result into the Lie group using the matrix exponential.

We now describe two other potential applications of Lie groups to geology: non-steady deformations and statistics of deformation tensors.

6.1. Non-steady homogeneous deformations

The matrix exponential framework of this paper opens up the possibility of viewing a deformation history as a path in a Lie group. The steady methods, on which we have focused throughout this paper, serve as building blocks for numerical methods on that Lie group. This approach may lead to improved precision in modeling non-steady deformations.

Consider the problem of characterizing deformation in a conglomerate (e.g., Hossack, 1968; Ramsay and Huber, 1983) using the shape preferred orientations (SPO) of clasts. Early workers typically assumed that clasts behave passively during deformation and therefore record bulk strain (e.g., Ramsay, 1967; Dunnet, 1969; Lisle, 1985). However, in some naturally deformed conglomerates, the clasts and matrix have different viscosities (e.g., Horsman et al., 2008; Czeck et al., 2009). As a consequence, the clasts do not deform passively, and assuming so leads to mis-estimation of strain (e.g., Gay, 1968; Meere et al., 2008).

Accounting for viscosity contrast in deforming clasts requires a more sophisticated model. For simplicity, assume that the host rock is deforming homogeneously and steadily, and that it contains a single ellipsoidal inclusion of different viscosity. The inclusion's deformation was described dynamically by Eshelby (1957, 1959) and Bilby et al. (1975). It is homogeneous but non-steady, being governed by $\dot{\vec{y}} = K\vec{y}$, where K depends on the inclusion's shape and orientation, and hence on time. That is, the velocity gradient tensor K and the ellipsoid tensor E (see Eq. (9)) interact over time to produce a complicated and subtle deformation history. Computing the final ellipsoid E (for comparison to SPO data) requires a numerical approximation, the details of which vary from author to author (e.g., Freeman, 1987; Jiang, 2007).

We propose that this problem could be solved by writing $E = \left(F^{-1}\right)^{\top} F^{-1}$ and treating F^{-1} using a numerical approximation method on the Lie group of homogeneous deformations (e.g., Munthe-Kaas, 1998). Fig. 10b illustrates our approach as a cartoon. We approximate the non-steady path as a sequence of steps (shown in green). Each step is steady in the sense of Eq. (1). Viewed in the Lie algebra, the approximation is a continuous path made of straight line segments. The matrix exponential sends this piecewise-linear path into the Lie group, producing an approximate deformation path that remains in the Lie group at all times. In contrast, a numerical approximation of F^{-1} as a mere 3×3 matrix (shown in orange) ignores the curved geometry of the Lie group within the set of 3×3 matrices, and hence leaves the Lie group.

For the deforming ellipsoid problem, this Lie group approach has two practical advantages. It automatically preserves the determinant, symmetry, and positive-definiteness of E, so that the simulated inclusion is always an ellipsoid of the correct volume, rather than a hyperboloid or other unphysical shape. Also, this approach seems to be highly precise (Munthe-Kaas, 1998). More development and testing is needed to evaluate its performance relative to the methods of Freeman (1987) and Jiang (2007), which do not use Lie groups explicitly but which do enjoy some of the same advantages. In any event, the Lie group view of deformation, which follows from the matrix exponential, reveals new possibilities for the modeling of SPO data and other non-steady geological problems.

6.2. Statistics of deformation tensors

Viewing finite deformations as elements of a Lie group opens up the possibility of doing statistics on that Lie group. To explain this idea, let us return to our analysis of Wallis (1992) from Section 5. Our goal in that section is not to criticize kinematic vorticity as a measure of deformation, or to suggest that general models should always be used in place of specialized ones. Rather, in demonstrating how models can be sensitive to choices made during the modeling process, we hope to encourage geologists to state their assumptions explicitly and to explore the effect of the assumptions on model results in their studies. The

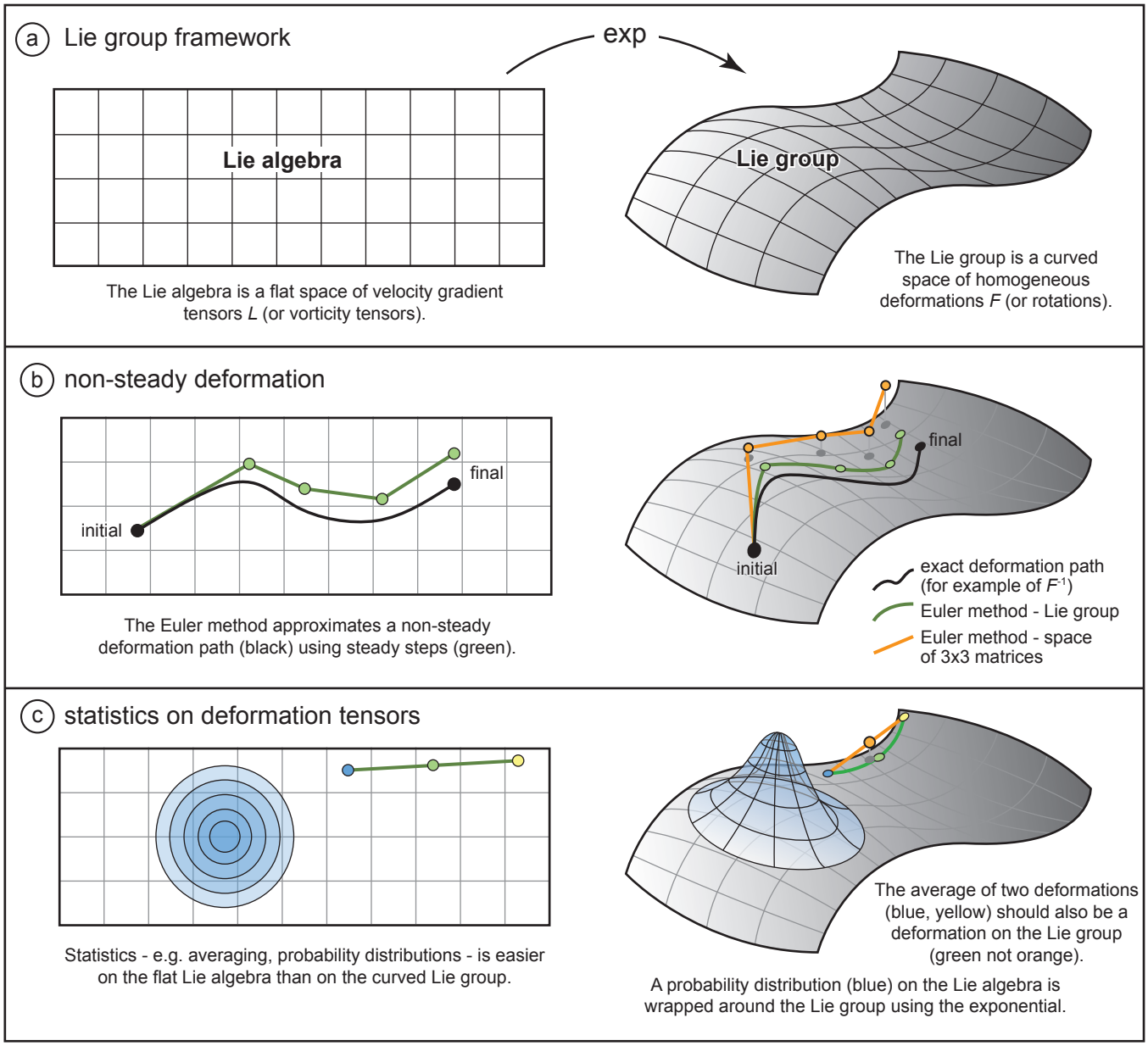

Figure 10: (a) The Lie algebra is "wrapped around" the Lie group by the matrix exponential. (b) The Lie algebra facilitates numerical methods for differential equations on the Lie group. A deformation path in the Lie group is shown in black. In the example of Section 6.1, this is the true path of F^{-1}. In the Lie algebra there is a corresponding path, also in black. Two approximations to this path are illustrated in green and orange. Each shows a series of steady steps denoted by the colored circles along each path. The green path remains in the Lie group throughout the approximation, and corresponds to a path with straight segments (i.e., steady steps) in the Lie algebra. The orange path accumulates more error than the green path, and in fact leaves the Lie group entirely. (c) Statistics on the Lie group may be more easily formulated on the Lie algebra.

best-fit process we describe can be used to test models with many degrees of freedom. However, it does not attempt to account for variation in the data, describe variation in the model parameters, indicate which model parameters are most useful for describing the data, etc.

This lack of statistical thoroughness or rigor seems to be common in structural geology modeling. The reason, we believe, is that structural geology data and concepts require advanced, differential-geometric statistical techniques. To do statistics with any kind of object, one must be able to define and integrate probability distributions over sets of that kind of object. In elementary statistics of a quantitative variable, for example, the data are real numbers and the statistics is formulated in terms of probability distributions on the set of real numbers. Structural geology relies upon many geometric concepts such as orientations of lines and planes, ellipsoidal markers, and deformation tensors. Statistics of structural geology data therefore requires sets of orientations, sets of ellipsoids, sets of deformation tensors, etc., over which we can integrate. In mathematics, these "sets of geometric objects" are often described in terms of Lie groups. Fig. 10c is a cartoon of this idea. It shows a probability distribution (in blue) on a Lie group, constructed by "pushing forward" a probability distribution on the Lie algebra.

Geology already employs some statistics of this kind. For example, directional and orientation statistics (Fisher, 1953; Downs, 1972; Mardia, 1972; Bingham, 1974; Cheeney, 1983; Borradaile, 2003; Tauxe, 2010) amount to statistics using Lie groups of rotations. Statistics of ellipsoids, which can also be viewed as statistics on a Lie group, have been applied to problems such as magnetic susceptibility (e.g., Borradaile, 2003; Tauxe, 2010).

Oertel (1981) took some preliminary steps toward a statistics of deformation tensors themselves. Starting from a set of finite strain ellipsoids, he first computed symmetric finite deformation tensors that explain them. He realized that it is not physically reasonable to average these tensors, but that it is reasonable to average infinitesimal deformation tensors, whose effects do approximately add. He used 1000th roots of the finite deformations as infinitesimal deformations, computed a mean and standard deviation for them, and performed a χ^2 test. However, he conceded that the assumptions of his analysis were uncertain, it was not clear whether the sample was large enough to support the conclusions, etc. In short, he lacked a rigorous statistical theory.

The Lie group framework clarifies Oertel's process. Because the Lie group is curved, the average of two or more finite deformation tensors (yellow and blue in Fig. 10c) may not be an element of the Lie group (as shown in orange). The infinitesimal deformations that Oertel computed are essentially approximations to velocity gradient tensors. Because the Lie algebra is flat, the velocity gradient tensors can be averaged (green), and the average can be "pushed forward" to the Lie group and taken as the average finite deformation. (See Appendix F for an example.)

In Sections 4 and 5, we present a unified, streamlined mathematical treatment of geological data and their kinematic modeling. The natural next step is to develop a unified, streamlined *statistical* treatment of these data and their associated kinematic models. Lie groups and their related spaces are an ideal setting for such a theory. In fact, much of the required mathematics has been constructed (e.g., Helgason, 1984; Wijsman, 1990; Murray and Rice, 1993), and researchers in other fields, such as medical imaging (e.g., Fletcher et al., 2004), are exploring similar avenues.

6.3. Conclusion

One could view the matrix exponential/logarithm framework as an ending — the final word, perhaps, on the solution of Eq. (1), one of the simplest differential equations in all of mathematics. We hope that the reader will regard exponentials and logarithms instead as a starting point — an invitation to investigate the application of Lie groups to geometric problems in structural geology.

7. Acknowledgements

We thank Scott Giorgis, Eric Horsman, Richard Jones, Gerhard Oertel, Mark Pearson, and Basil Tikoff for helpful discussions about the ideas in this manuscript; Eric and Richard are also thanked for instructive comments on an earlier draft. We thank reviewers Haakon Fossen and Kieran Mulchrone for comments that improved the manuscript, and associate editor William Dunne for his guidance. Funding support from the Carleton College Class of '49 Fellowship (Titus) was invaluable for providing the time necessary to complete this manuscript.

8. References

Allmendinger, R.W., Loveless, J.P., Pritchard, M.E., Meade, B., 2009. From decades to epochs; spanning the gap between geodesy and structural geology of active mountain belts. Journal of Structural Geology 31, 1409–1422.

Allmendinger, R.W., Relinger, R., Loveless, J.P., 2007. Strain and rotation rate from GPS in Tibet, Anatolia, and the Altiplano. Tectonics 26, doi:10.1029/2006TC002030.

Angelier, J., Colletta, B., Anderson, R.E., 1985. Neogene paleostress changes in the Basin and Range: A case study at Hoover Dam, Nevada-Arizona. Geological Society of America Bulletin 96, 347–361.

Anglier, J., 1994. Fault slip analysis and palaeostress reconstruction, in: Hancock, P. (Ed.), Continental Deformation. Pergamon press, Oxford, pp. 53–100.

Bailey, C.M., Eyster, E.L., 2003. General shear deformation in the Pinaleño Mountains metamorphic core complex, Arizona. Journal of Structural Geology 25, 1883–1892.

Baird, G.B., Hudleston, P.J., 2007. Modeling the influence of tectonic extrusion and volume loss on the geometry, displacement, vorticity, and strain compatibility of ductile shear zones. Journal of Structural Geology 29, 1665–1678.

Belinfante, J.G., Kolman, B., 1972. A Survey of Lie Groups and Lie Algebras with Applications and Computational Methods. Society for Industrial and Applied Mathematics, Philadelphia.

Bell, A., 1979. Factorization of finite strains in three dimensions — a computer method. Journal of Structural Geology 1, 163–167.
Bergerat, F., 1987. Stress fields in the European platform at the time of Africa-Eurasia collision. Tectonics 6, 99–132.
Bhattacharyya, P., Hudleston, P., 2001. Strain in ductile shear zones in the Caledonides of northern Sweden; a three-dimensional puzzle. Journal of Structural Geology 23, 1549–1565.
Bilby, B., Eshelby, J., Kundu, A., 1975. The change of shape of a viscous ellipsoidal region embedded in a slowly deforming matrix having a different viscosity. Tectonophysics 28, 265–274.
Bingham, C., 1974. An antipodally symmetric distribution on the sphere. Annals of Statistics 2, 1201–1225.
Biot, M.A., 1961. Theory of folding of stratified viscoelastic media and is implication in tectonics an orogenesis. Geological Society of America Bulletin 72, 1595–1620.
Bird, P., 2002. Stress direction history of the western United States and Mexico since 85 Ma. Tectonics 21, doi: 10.1029/2001TC001319.
Bobyarchick, A., 1986. The eigenvalues of steady flow in Mohr space. Tectonophysics 122, 35–51.
Borradaile, G.J., 2003. Statistics of Earth Science Data. Springer-Verlag, Berlin.
Cheeney, R.F., 1983. Statistical Methods in Geology. George Allen & Unwin, London.
Clegg, P., Holdsworth, R.E., 2005. Complex deformation as a result of strain partitioning in transpression zones; an example from the Leinster Terrane, SE Ireland. Journal of the Geological Society of London 162, 187–202.
Cloos, E., 1947. Oölite deformation in the South Mountain fold, Maryland. Geological Society of America Bulletin 58, 843–917.
Cobbold, P.R., Cosgrove, J.W., Summers, J.M., 1971. Development of internal structures in deformed anisotropic rocks. Tectonophysics 12, 23–53.
Coward, M.P., 1976. Strain within ductile shear zones. Tectonophysics 34, 181–197.
Culver, W.J., 1966. On the existence and uniqueness of the real logarithm of a matrix. Proc. of the Amer. Math. Soc. 17, 1146–1151.
Curtis, M.L., 1984. Matrix Groups. Springer-Verlag, New York. 2nd edition.
Czeck, D., Fissler, D., Horsman, E., Tikoff, B., 2009. Strain analysis and rheology contrasts in polymictic conglomerates: An example from the Seine metaconglomerates, Superior Province, Canada. Journal of Structural Geology 31, 1365–1376.
Czeck, D., Hudleston, P., 2004. Physical experiments of vertical transpression with localized nonvertical extrusion. Journal of Structural Geology 26, 573–581.
Czeck, D.M., Hudleston, P.J., 2003. Testing models for obliquely plunging lineations in transpression; a natural example and theoretical discussion. Journal of Structural Geology 25, 959–982.
De Paor, D.G., 1981. A new technique of strain analysis using three-dimensional distributions of passively deformed linear markers. Tectonophysics 76, T13–T16.
De Paor, D.G., 1983. Orthographic analysis of geological structures I. Deformation theory. Journal of Structural Geology 5, 255–277.
De Paor, D.G., 1986. Orthographic analysis of geological structures II. Practical applications. Journal of Structural Geology 8, 87–100.
Dewey, J., 2002. Transtension in arcs and orogens. International Geology Review 44, 402–439.
Dias, R., Ribeiro, A., 1994. Constriction in a transpressive regime: an example in the Iberian branch of the Ibero-Armorican arc. Journal of Structural Geology 16, 1543–1554.
Downs, T., 1972. Orientation statistics. Biometrika 59, 665–676.
Dunlap, W.J., Hirth, G., Teyssier, C., 1997. Thermomechanical evolution of a ductile duplex. Tectonics 16, 983–1000.
Dunnet, D., 1969. A technique of finite strain analysis using elliptical particles. Tectonophysics 7, 117–136.
Elliott, D., 1970. Determination of finite strain and initial shape from deformed elliptical objects. Geological Society of America Bulletin 81, 2221–2236.
Elliott, D., 1972. Deformation paths in structural geology. Geological Society of America Bulletin 83, 2621–2638.
Eshelby, J., 1957. The determination of the elastic field of an ellipsoidal inclusion, and related problems. Proceedings of the Royal Society of London A241, 376–396.
Eshelby, J., 1959. The elastic field outside an ellipsoidal inclusion. Proceedings of the Royal Society of London A252, 561–569.
Etheridge, M.A., Wall, V.J., Vernon, R.H., 1983. The role of the fluid phase during regional metamorphism and deformation. Journal of Metamorphic Geology 1, 205–226.
Evans, M., Dunne, W., 1991. Strain factorization and partitioning in the North Mountain thrust sheet, central Appalachians, U.S.A. Journal of Structural Geology 13, 21–36.
Faure, M., 1985. Microtectonic evidence for eastward ductile shear in the Jurassic orogen of SW Japan. Journal of Structural Geology 7, 175–186.
Fefferman, C.L., 2006. Existence and smoothness of the Navier-Stokes equation, in: Carlson, J., Jaffe, A., Wiles, A. (Eds.), The Millennium Prize Problems. American Mathematical Society, Providence, R.I., pp. 57–70.
Fernández, C., Díaz-Azpiroz, M., 2009. Triclinic transpression zones with inclined extrusion. Journal of Structural Geology 31, 1255–1269.
Fisher, R., 1953. Dispersion on a sphere. Proceedings of the Royal Society of London 217, 295–305.
Fletcher, P.T., Lu, C., Pizer, S.M., Joshi, S.C., 2004. Principal geodesic analysis for the study of nonlinear statistics of shape. IEEE Trans. Med. Imaging 23, 995–1005.
Flinn, D., 1979. The deformation matrix and the deformation ellipsoid. Journal of Structural Geology 1, 299–307.
Fossen, H., 2010. Structural Geology. Cambridge University Press, Cambridge.
Fossen, H., Tikoff, B., 1993. The deformation matrix for simultaneous simple shearing, pure shearing and volume change, and its application to transpression-transtension tectonics. Journal of Structural Geology 15, 413–422.
Freeman, B., 1987. The behavior of deformable ellipsoidal particles in three-dimensional slow flows: implications for geological strain analysis. Tectonophysics 132, 297–309.
Gantmacher, F.R., 1959. The Theory of Matrices. Chelsea Pub. Co., New York.
Gay, N., 1968. Pure shear and simple shear deformation of inhomogeneous viscous fluids. 2. The determination of the total finite strain in a rock from objects such as deformed pebbles. Tectonophysics 5, 295–302.
Ghosh, S.K., 2001. Types of transpressional and transtensional deformation, in: Koyi, H.A., Mancktelow, N.S. (Eds.), Tectonic Modeling: A volume in honor of Hans Ramberg. Geological Society of America Memoir 193, Boulder, CO, pp. 1–20.
Ghosh, S.K., Ramberg, H., 1976. Reorientation of inclusions by combination of pure and simple shear. Tectonophysics 34, 1–70.
Gilmore, R., 1974. Lie Groups, Lie Algebras, and Some of Their Applications. John Wiley & Sons, New York.
Giorgis, S., Markley, M., Tikoff, B., 2004. Vertical axis rotation of rigid crustal blocks driven by mantle flow, in: Grocott, J., McCaffrey, K., Taylor, G., Tikoff, B. (Eds.), Vertical Coupling and Decoupling in the Lithosphere. Geological Society, London. volume 227, pp. 83–100.
Giorgis, S., Tikoff, B., 2004. Constraints on kinematics and strain from feldspar porphyroclast populations, in: Alsop, I., Holdsworth, R., McCaffery, K. (Eds.), Transport and Flow Processes in Shear Zones. Geological Society, London. volume 224, pp. 265–285.
Goldstein, A., Knight, J., Kimball, K., 1999. Deformed graptolites, finite strain and volume loss during cleavage formation in rocks of the Taconic slate belt, New York and Vermont, U.S.A. Journal of Structural Geology 20, 1769–1782.
Goodwin, L.B., Tikoff, B., 2002. Competency contrast, kinematics, and the development of foliations and lineations in the crust. Journal of Structural Geology 24, 1065–1085.
Goodwin, L.B., Williams, P.F., 1996. Deformation path partitioning

within a transpressive shear zone, Marble Cove, Newfoundland. Journal of Structural Geology 18, 975–990.
Grasemann, B., Fritz, H., Vannay, J.C., 1999. Quantitative kinematic flow analysis from the Main Central Thrust Zone (NW-Himalaya, India): Implications for a decelerating strain path and the extrusion of orogenic wedges. Journal of Structural Geology 21, 837–853.
Gudmundsson, A., 1990. Dyke emplacement at divergent plate boundaries, in: Parker, A.J., Rickwood, P.C., Tucker, D.H. (Eds.), Mafic Dykes and Emplacement Mechanisms. Balkema, Rotterdam, pp. 47–62.
Hall, B.C., 2003. Lie groups, Lie algebras, and representations. Springer-Verlag, New York.
Halmos, P.R., 1958. Finite-Dimensional Vector Spaces. D. Van Nostrand, Princeton, New Jersey. 2nd edition.
Harding, T.P., 1973. The Newport-Inglewood trend, California—an example of wrenching style of deformation. Bulletin of the American Association of Petroleum Geologists 57, 97–116.
Helgason, S., 1984. Groups and Geometric Analysis. Academic Press, Orlando, Florida.
Higham, N.J., 2008. Functions of Matrices: Theory and Computation. Society for Industrial and Applied Mathematics.
Hoffman, K., Kunze, R., 1961. Linear Algebra. Prentice-Hall, Englewood Cliffs, New Jersey.
Horsman, E., Tikoff, B., 2005. Quantifying simultaneous discrete and distributed deformation. Journal of Structural Geology 27, 1168–1189.
Horsman, E., Tikoff, B., 2007. Constraints on deformation path from finite strain gradients. Journal of Structural Geology 29, 256–272.
Horsman, E., Tikoff, B., Czeck, D., 2008. Rheological implications of heterogeneous deformation at multiple scales in the Late Cretaceous Sierra Nevada, California. Geological Society of America Bulletin 120, 238–255.
Hossack, J., 1968. Pebble deformation and thrusting in the Bygdin area (southern Norway). Tectonophysics 5, 315–339.
Hudleston, P.J., Schultz-Ela, D., Southwick, D., 1988. Transpression in an Archean greenstone belt, northern Minnesota. Canadian Journal of Earth Sciences 25, 1060–1068.
Iacopini, D., Carosi, R., Xypolias, P., 2010. Implications of complex eigenvalues in homogeneous flow: A three-dimensional kinematic analysis. Journal of Structural Geology 32, 93–106.
Iacopini, D., Passchier, C.W., Koehn, D., Carosi, R., 2007. Fabric attractors in general triclinic flow systems and their application to high strain shear zones; a dynamical system approach. Journal of Structural Geology 29, 298–317.
Jeffery, G.B., 1922. The motion of ellipsoidal particles immersed in a viscous fluid. Proceedings of the Royal Society of London A102, 161–179.
Jessup, M.J., Law, R.D., Frassi, C., 2007. The Rigid Grain Net (RGN): an alternative method for estimating mean kinematic vorticity number (W_{m}). Journal of Structural Geology 29, 411–421.
Jiang, D., 1994. Vorticity determination, distribution, partitioning and the heterogeneity and non-steadiness of natural deformations. Journal of Structural Geology 16, 121–130.
Jiang, D., 1999. Vorticity decomposition and its application to sectional flow characterization. Tectonophysics 301, 243–259.
Jiang, D., 2007. Numerical modeling of the motion of deformable ellipsoidal objects in slow viscous flows. Journal of Structural Geology 29, 435–452.
Jiang, D., White, J.C., 1995. Kinematics of rock flow and the interpretation of geological structures, with particular reference to shear zones. Journal of Structural Geology 17, 1249–1265.
Jiang, D., Williams, P.F., 1998. High-strain zones; a unified model. Journal of Structural Geology 20, 1105–1120.
Jones, R.R., Holdsworth, R.E., 1998. Oblique simple shear in transpression zones, in: Holdsworth, R.E., Strachan, R.A., Dewey, J.F. (Eds.), Continental Transpressional and Transtensional Tectonics. Geological Society, London. volume 135, pp. 35–40.
Jones, R.R., Holdsworth, R.E., Clegg, P., McCaffrey, K., Tavarnelli, E., 2004. Inclined transpression. Journal of Structural Geology 26, 1531–1548.
Kenney, C., Laub, A.J., 1989. Condition estimates for matrix functions. SIAM J. Matrix Anal. & Appl. 10, 191–209.
Koehn, D., Renard, F., Toussaint, R., Passchier, C., 2007. Growth of stylolite teeth patterns depending on normal stress and finite compaction. Earth and Planetary Science Letters 257, 582–595.
Kumerics, C., Ring, U., Brichau, S., Glodny, J., Monié, P., 2005. The extensional Messaria shear zone and associated brittle detachment faults, Aegean Sea, Greece. Journal of the Geological Society of London 162, 701–721.
Lamb, S., 1994a. A simple method for estimating the horizontal velocity field in wide zones of active deformation - I. Description, with an example from California. Geophysical Journal International 119, 297–312.
Lamb, S., 1994b. A simple method for estimating the horizontal velocity field in wide zones of active deformation - II. Examples from New Zealand, Central Asia and Chile. Geophysical Journal International 119, 313–337.
Law, R.D., Knipe, R.J., Dayan, H., 1984. Strain path partitioning within thrust sheets: microstructural and petrofabric evidence from the Moine Thrust zone at Loch Eriboll, northwest Scotland. Journal of Structural Geology 6, 477–497.
Law, R.D., Searle, M.P., Simpson, R.L., 2004. Strain, deformation temperatures and vorticity of flow at the top of the Greater Himalayan Slab, Everest Massif, Tibet. Journal of the Geological Society of London 161, 305–320.
Lay, D.C., 1994. Linear Algebra and Its Applications. Addison Wesley, Reading, Massachusetts.
Lin, S., Jiang, D., Williams, P.F., 1998. Transpression (or transtension) zones of triclinic symmetry; natural example and theoretical modelling, in: Holdsworth, R.E., Strachan, R.A., Dewey, J.F. (Eds.), Continental Transpressional and Transtensional Tectonics. Geological Society, London. volume 135, pp. 41–57.
Lisle, R.J., 1977. Estimation of the tectonic strain ratio from the mean shape of deformed elliptical markers. Geologie en Mijnbouw 56, 140–144.
Lisle, R.J., 1985. Geological Strain Analysis: A Manual for the R_f/ϕ Technique. Pergamon Press, Oxford.
Lister, G., Hobbs, B., 1980. The simulation of fabric development during plastic deformation and its application to quartzite: the influence of deformation history. Journal of Structural Geology 2, 355–370.
Lister, G., Williams, P., 1979. Fabric development in shear zones: Theoretical controls and observed phenomena. Journal of Structural Geology 1, 283–297.
Lister, G., Williams, P., 1983. The partitioning of deformation in flowing rock masses. Tectonophysics 92, 1–33.
Malvern, L., 1969. Introduction to the Mechanics of a Continuous Medium. Prentice-Hall, Englewood Cliffs, N.J.
Mardia, K., 1972. Statistics of Directional Data. Academic Press, New York.
Markley, M., Wojtal, S., 1996. Mesoscopic structure, strain, and volume loss in folded cover strata, Valley and Ridge Province, Maryland. American Journal of Science 296, 23–57.
Matthews, P.E., Bond, R.A.B., Van den Berg, J.J., 1974. An algebraic method of strain analysis using elliptical markers. Tectonophysics 24, 31–67.
McKenzie, D., 1979. Finite deformation during fluid flow. Geophysical Journal of the Royal Astronomical Society 58, 689–715.
McKenzie, D., Jackson, J., 1983. The relationship between strain rates, crustal thickening, palaeomagnetism, finite strain and fault movements within a deforming zone. Earth and Planetary Science Letters 65, 182–202.
Means, W.D., 1976. Stress and Strain. Springer-Verlag, New York.
Means, W.D., 1994. Rotational quantities in homogeneous flow and the development of small-scale structure. Journal of Structural Geology 16, 437–445.
Means, W.D., Hobbs, B.E., Lister, G.S., Williams, P.F., 1980. Vorticity and non-coaxiality in progressive deformations. Journal of Structural Geology 2, 371–378.
Meere, P.A., Mulchrone, K.F., Sears, J.F., Bradway, M.D., 2008. The effect of non-passive clast behaviour in the estimation of finite

strain in sedimentary rocks. Journal of Structural Geology 30, 1264–1271.
Moler, C., Van Loan, C., 2003. Nineteen dubious ways to compute the exponential of a matrix, twenty-five years later. Society for Industrial and Applied Mathematics Review 45, 1–46.
Mookerjee, M., Mitra, G., 2009. Understanding kinematic data from the Moine thrust zone in terms of a kinematics-based mathematical model of deforming thrust wedges. Journal of Structural Geology 31, 1556–1572.
Mulchrone, K.F., 2002. A statistic for estimating strain with confidence intervals from deformed line distributions with an application to schists and gneisses of the Western Gneiss Region, west central Norway. Journal of Structural Geology 24, 545–556.
Munson, B.R., Young, D.F., Okiishi, T.H., Huebsch, W.W., 2009. Fundamentals of Fluid Mechanics. John Wiley & Sons. 6th edition.
Munthe-Kaas, H., 1998. Runge-Kutta methods on Lie groups. BIT 38, 92–111.
Murray, M.K., Rice, J.W., 1993. Differential Geometry and Statistics. Chapman & Hall, London.
Nemcock, M., Lisle, R., 1995. A stress inversion procedure for polyphase fault/slip data. Journal of Structural Geology 17, 1445–1453.
Neves, S.P., da Silva, J.M.R., Mariano, G., 2005. Oblique lineations in orthogneisses and supracrustal rocks; vertical partitioning of strain in a hot crust; eastern Borborema Province, NE Brazil. Journal of Structural Geology 27, 1513–1527.
Nicolas, A., 1989. Structures of Ophiolites and Dynamics of Oceanic Lithosphere. Kluwer Academic Publishers, Dordrecht.
Nissen, H.U., 1964. Dynamic and kinematic analysis of deformed crinoid stems in a quartz graywacke. Journal of Geology 72, 346–360.
Oertel, G., 1981. Strain estimation from scattered observations in an inhomogeneously deformed domain of rocks. Tectonophysics 77, 133–150.
Oertel, G., Reymer, A.P.S., 1992. Perturbations of strain and rotation in a nodular slate. Journal of Structural Geology 14, 257–269.
Panozzo, R.H., 1984. Two-dimensional strain from the orientation of lines in a plane. Journal of Structural Geology 6, 215–221.
Passchier, C.W., 1987a. Efficient use of the velocity gradients tensor in flow modelling. Tectonophysics 136, 159–163.
Passchier, C.W., 1987b. Stable positions of rigid objects in noncoaxial flow; a study in vorticity analysis. Journal of Structural Geology 9, 679–690.
Passchier, C.W., 1988a. Analysis of deformation paths in shear zones. Geologische Rundschau 77, 309–318.
Passchier, C.W., 1988b. The use of Mohr circles to describe noncoaxial progressive deformation. Tectonophysics 149, 323–338.
Passchier, C.W., 1990. A Mohr circle construction to plot the stretch history of material lines. Journal of Structural Geology 12, 513–515.
Passchier, C.W., 1997. The fabric attractor. Journal of Structural Geology 19, 113–127.
Passchier, C.W., 1998. Monoclinic model shear zones. Journal of Structural Geology 20, 1121–1137.
Passchier, C.W., Urai, J.L., 1988. Vorticity and strain analysis using Mohr diagrams. Journal of Structural Geology 10, 755–763.
Pavlis, T., 1986. The role of strain heating in the evolution of megathrusts. Journal of Geophysical Research 91, 6522–6534.
Petit, J.P., Mattauer, M., 1995. Paleostress superimposition deduced from structures in limestone: The Matelles exposure, Languedoc, France. Journal of Structural Geology 17, 245–256.
Platt, J., Behrmann, J., 1986. Structures and fabrics in a crustal scale shear zone, Betic Cordilleras, S.E. Spain. Journal of Structural Geology 8, 15–34.
Platt, J., Vissers, R., 1980. Extensional structures in anisotropic rocks. Journal of Structural Geology 2, 397–410.
Platt, J.P., 1984. Secondary cleavages in ductile shear zones. Journal of Structural Geology 6, 439–442.
Pollard, D., Segall, P., Delaney, P., 1982. Formation and interpretation of dilatant echelon cracks. Geological Society of America Bulletin 93, 1291–1303.
Pollard, D.D., Fletcher, R.C., 2005. Fundamentals of Structural Geology. Cambridge Univ. Press, Cambridge.
Pollatsek, H., 2009. Lie Groups: A Problem-Oriented Introduction via Matrix Groups. Mathematical Association of America.
Provost, A., Buisson, C., Merle, O., 2004. From progressive to finite deformation and back. Journal of Geophysical Research 109, doi:10.1029/2001JB001734.
Ramberg, H., 1975. Particle paths, displacement and progressive strain applicable to rocks. Tectonophysics 28, 1–37.
Ramsay, J.G., 1967. Folding and fracturing of rocks. McGraw-Hill, New York.
Ramsay, J.G., Graham, R.H., 1970. Strain variation in shear belts. Canadian Journal of Earth Sciences 7, 786–813.
Ramsay, J.G., Huber, M.I., 1983. The Techniques of Modern Structural Geology. Academic Press, London.
Ring, U., 1998. Volume strain, strain type and flow path in a narrow shear zone. Geologische Rundschau 86, 786–801.
Robin, P.Y., Cruden, A.R., 1994. Strain and vorticity patterns in ideally ductile transpression zones. Journal of Structural Geology 16, 447–466.
Sanderson, D.J., 1977. The analysis of finite strain using lines with an initial random orientation. Tectonophysics 43, 199–211.
Sanderson, D.J., Marchini, W.R.D., 1984. Transpression. Journal of Structural Geology 6, 449–458.
Sarkarinejad, K., Azizi, A., 2008. Slip partitioning and inclined dextral transpression along the Zagros thrust system, Iran. Journal of Structural Geology 30, 116–136.
Short, H.A., Johnson, S.E., 2006. Estimation of vorticity from fibrous calcite veins, central Maine, USA. Journal of Structural Geology 28, 1167–1182.
Siddans, A.W.B., 1980a. Analysis of three-dimensional, homogeneous, finite strain using ellipsoidal objects. Tectonophysics 64, 1–16.
Siddans, A.W.B., 1980b. Elliptical markers and non-coaxial strain increments. Tectonophysics 67, T21–T25.
Simpson, C., De Paor, D.G., 1993. Strain and kinematic analysis in general shear zones. Journal of Structural Geology 15, 1–20.
Simpson, C., De Paor, D.G., 1997. Practical analysis of general shear zones using porphyroclast hyperbolic distribution method: An example from the Scandianvian Caledonides, in: Sengupta, S. (Ed.), Evolution of Geological Structures in Micro- to Macroscales. Chapman and Hall, London, pp. 169–184.
Soto, J.I., 1997. A general deformation matrix for three-dimensions. Mathematical Geology 29, 93–130.
Srivastava, D.C., Shah, J., 2006. Digital method for strain estimation and retrodeformation of bilaterally symmetric fossils. Geology 34, 593–596.
Srivastava, H.B., Hudleston, P., Earley, Drummond, I., 1995. Strain and possible volume loss in a high-grade ductile shear zone. Journal of Structural Geology 17, 1217–1231.
Sullivan, W.A., Law, R.D., 2007. Deformation path partitioning within the transpressional White Mountain shear zone, California and Nevada. Journal of Structural Geology 29, 583–598.
Sylvester, A.G., Smith, R.R., 1976. Tectonic transpression and basement-controlled deformation in San Andreas fault zone, Salton trough, California. Bulletin of the American Association of Petroleum Geologists 60, 2081–2102.
Talbot, C.J., 1970. The minimum strain ellipsoid using deformed quartz veins. Tectonophysics 9, 47–67.
Tan, B.K., 1973. Determination of strain ellipses from deformed ammonoids. Tectonophysics 16, 89–101.
Tauxe, L., 2010. Essentials of Paleomagnetism. University of California Press.
Tavarnelli, E., Holdsworth, R.E., Clegg, P., Jones, R.R., McCaffrey, K.J.W., 2004. The anatomy and evolution of a transpressional imbricate zone, Southern Uplands, Scotland. Journal of Structural Geology 26, 1341–1360.
Teyssier, C., Tikoff, B., 1999. Fabric stability in oblique convergence and divergence. Journal of Structural Geology 21, 969–974.
Tikoff, B., Fossen, H., 1993. Simultaneous pure and simple shear;

the unifying deformation matrix. Tectonophysics 217, 267–283.
Tikoff, B., Fossen, H., 1995. The limitations of three-dimensional kinematic vorticity analysis. Journal of Structural Geology 17, 1771–1784.
Tikoff, B., Teyssier, C., 1994. Strain modeling of displacement-field partitioning in transpressional orogens. Journal of Structural Geology 16, 1575–1588.
Titus, S.J., Dyson, M., DeMets, C., Tikoff, B., Rolandone, F., Bürgmann, R., 2011. Geologic versus geodetic deformation adjacent to the San Andreas fault, central California. Geological Society of America Bulletin doi:10.1130/B30150.1.
Titus, S.J., Housen, B., Tikoff, B., 2007. A kinematic model for the Rinconada fault system in central California based on structural analysis of en echelon folds and paleomagnetism. Journal of Structural Geology 29, 961–982.
Trotter, H., 1959. Product of semigroups of operators. Proc. of the Amer. Math. Soc. 10, 545551.
Truesdell, C.A., 1953. Two measures of vorticity. Journal of Rational Mechanics Analysis 2, 173–217.
Twiss, R., Moores, E., 2007. Structural Geology. W. H. Freeman and Co., New York.
Twiss, R., Unruh, J., 1998. Analysis of fault slip inversions: Do they constrain stress or strain rate? Journal of Geophysical Research 103, 12205–12222.
Vissers, R., 1989. Asymmetric quartz c-axis fabrics and flow vorticity: A study using rotated garnets. Journal of Structural Geology 11, 231–244.
Vitale, S., Mazzoli, S., 2009. Finite strain analysis of a natural ductile shear zone in limestones; insights into 3-D coaxial vs. noncoaxial deformation partitioning. Journal of Structural Geology 31, 104–113.
Wallis, S.R., 1992. Vorticity analysis in a metachert from the Sanbagawa Belt, SW Japan. Journal of Structural Geology 14, 271–280.
Wallis, S.R., 1995. Vorticity analysis and recognition of ductile extension in the Sanbagawa belt, SW Japan. Journal of Structural Geology 17, 1077–1093.
Wang, T., Pei, X., Wang, X., Hu, N., Li, W., Zhang, G., 2005. Orogen-parallel westward oblique uplift of the Qinling basement complex in the core of the Qinling Orogen (China); an example of oblique extrusion of deep-seated metamorphic rocks in a collisional orogen. Journal of Geology 113, 181–200.
Weijermars, R., 1992. Progressive deformation in anisotropic rocks. Journal of Structural Geology 14, 723–742.
Weil, A.B., Yonkee, A., Sussman, A., 2010. Reconstructing the kinematic evolution of curved mountain belts: A paleomagnetic study of Triassic red beds from the Wyoming salient, Sevier thrust belt, U.S.A. Geological Society of America Bulletin 122, 3–23.
Whitney, D.L., Teyssier, C., Heizler, M.T., 2007. Gneiss domes, metamorphic core complexes, and wrench zones: Thermal and structural evolution of the Niğde Massif, central Anatolia. Tectonics 26, 1315–1343.
Wijsman, R.A., 1990. Invariant Measures on Groups and Their Use in Statistics. Institute of Mathematical Statistics, Hayward, California.
Wilcox, R.E., Harding, T.P., Seely, D.R., 1973. Basic wrench tectonics. Bulletin of the America Association of Petroleum Geologists 57, 74–96.
Wright, T.O., Platt, L.B., 1982. Pressure dissolution and cleavage in the Martinsburg Shale. American Journal of Science 282, 122–135.
Xypolias, P., 2010. Vorticity analysis in shear zones: A review of methods and applications. Journal of Structural Geology 32, 2072–2092.
Xypolias, P., Koukouvelas, I.K., 2001. Kinematic vorticity and strain rate patterns associated with ductile extrusion in the Chelmos shear zone (external Hellenides, Greece). Tectonophysics 338, 59–77.
Yonkee, A., 2005. Strain patterns within part of the Willard thrust sheet, Idaho-Utah-Wyoming thrust belt. Journal of Structural Geology 27, 1315–1343.
Zhang, G., Hynes, A., 1995. Determination of position-gradient tensor from strain measurements and its implications for the displacement across a shear zone. Journal of Structural Geology 17, 1587–1599.
Zoback, M., 1992. First- and second-order patterns of stress in the lithosphere: The World Stress Map Project. Journal of Geophysical Research 97, 11,703–11,728.
Zoback, M., Moss, D., Mastin, L., Anderson, R., 1985. Wellbore breakouts and in situ stress. Journal of Geophysical Research 90, 5523–5530.
Zoback, M., Zoback, M., 1980. State of stress in the conterminous U.S. Journal of Geophysical Research 85, 6113–6156.

Appendix A. Matrix decompositions

In this section we review the Jordan, Schur, and singular value decompositions. We then use the decompositions to evaluate the generality of earlier models of deformation by Tikoff and Fossen (1993) and Soto (1997).

A *Jordan block* is a square matrix with a single value λ repeated along its diagonal, 1s immediately above the diagonal, and 0s elsewhere:

$$\left[\ \lambda\ \right], \quad \begin{bmatrix} \lambda & 1 \\ 0 & \lambda \end{bmatrix}, \quad \begin{bmatrix} \lambda & 1 & 0 \\ 0 & \lambda & 1 \\ 0 & 0 & \lambda \end{bmatrix}, \quad \ldots.$$

A *Jordan matrix* is a matrix comprising Jordan blocks along its diagonal, such as

$$\begin{bmatrix} \lambda_1 & 1 & 0 \\ 0 & \lambda_1 & 0 \\ 0 & 0 & \lambda_2 \end{bmatrix}$$

(which has a 2×2 block and a 1×1 block).

Any square matrix A can be decomposed as $A = PJP^{-1}$, where P is a change-of-basis matrix and J is a Jordan matrix. This is called the *Jordan decomposition* of A (e.g., Halmos, 1958; Hoffman and Kunze, 1961). The matrix J, which is unique up to permutations of its Jordan blocks, is called the *Jordan canonical form* of A. The change-of-basis matrix P is not unique, because it can be replaced with PS, where S is any matrix satisfying $SJS^{-1} = J$.

An important special case occurs when all of the blocks in J are 1×1. For then J is diagonal, and Jordan decomposition is simply diagonalization. There is a precise mathematical sense in which *almost all matrices are diagonalizable*. A nondiagonalizable matrix is not numerically stable, as an arbitrarily small perturbation to the entries will, with probability 1, make the matrix diagonalizable. This characteristic makes the Jordan decomposition inappropriate for matrices derived from empirical data. However, geologists frequently use nondiagonalizable matrices to develop models — simple shear being the archetype — and we continue the tradition in this paper.

This paper also uses the *Schur decomposition* (e.g., Lay, 1994), which comes in several flavors. First, any complex square matrix A can be written as a product $A = QUQ^{-1}$ of complex matrices, where U is upper-triangular and $Q^{-1} = \bar{Q}^\top$. Second, if A is real and has only real eigenvalues, then a real Q and U can be found; that is, $A = QUQ^{-1}$, where U is real upper-triangular and Q is orthogonal. This is a *real Schur decomposition*. Schur decompositions are not unique. For example, if $A = QUQ^\top$ is a real Schur decomposition, then so is $A = Q'U'Q'^\top$, where

$$Q' = Q \begin{bmatrix} 1 & 0 & 0 \\ 0 & 1 & 0 \\ 0 & 0 & -1 \end{bmatrix},$$

$$U' = \begin{bmatrix} U_{11} & U_{12} & -U_{13} \\ 0 & U_{22} & -U_{23} \\ 0 & 0 & U_{33} \end{bmatrix}.$$

Notice that $\det Q' = -\det Q$; therefore either Q or Q' is a rotation. In summary, a real A with real eigenvalues always has a real Schur decomposition $A = QUQ^\top$ in which Q is a rotation and U is real upper-triangular; we call this a *rotational Schur decomposition* in this paper.

Schur decomposition enjoys two advantages over Jordan decomposition. First, it is numerically robust (Moler and Van Loan, 2003). Second, it uses only orthogonal changes of basis, which are often more convenient than arbitrary changes of basis. The disadvantage of Schur decomposition is that the upper-triangular matrix U is not as simple as the Jordan canonical form J.

The third decomposition used in this paper is the *singular value decomposition* (e.g., Lay, 1994; Provost et al., 2004): For any real square matrix F there exist orthogonal matrices Q and R and a diagonal matrix D, such that all entries of D are nonnegative real and $F = QDR$.

These decompositions are computed in *MATLAB* by `jordan`, `schur`, and `svd`, in *Mathematica* by `JordanDecomposition`, `SchurDecomposition`, and `SingularValueDecomposition`, and in *Maple* by `JordanForm`, `SchurForm`, and `Svd`.

The Schur decomposition illuminates the kinematic model of Tikoff and Fossen (1993). They described deformations arising from an arbitrary upper-triangular velocity gradient tensor. But any real-eigenvalue L can be written, via the rotational Schur decomposition, as $L = QUQ^\top$, where Q is a rotation and U is upper-triangular. It follows that the progressive deformation tensor is

$$\exp tL = \exp t\left(QUQ^\top\right) = Q\left(\exp tU\right)Q^\top.$$

By computing $\exp tU$ for any U, Tikoff and Fossen (1993) effectively computed $\exp tL$ for any real-eigenvalue L. Their method does not address L with non-real eigenvalues.

Soto (1997) described deformations arising from velocity gradient tensors of the form

$$L = R^\top NR + D,$$

where R is a rotation, N is strictly upper-triangular, and D is diagonal. This model includes that of Tikoff and Fossen (1993) as a special case when R is the identity tensor. If we allow for rotational changes of coordinates then Soto's model handles *all* L. That is, for every 3×3 matrix L there exist a rotation R, a strictly upper-triangular N, and a diagonal D, such that

$$L = N + RDR^\top = R\left(R^\top NR + D\right)R^\top.$$

(Given an L, define a matrix A by $A_{ij} = L_{ij}$ if $i \geq j$, $A_{ij} = L_{ji}$ if $i < j$. Then A is symmetric, so it can be diagonalized by a rotational change of basis: $A = RDR^\top$. Let $N = L - A$. Then N is strictly upper-triangular and

$L = N + RDR^\top$.) On the other hand, if we do not allow for additional rotational changes of coordinates then Soto's model is not fully general. For example, for

$$L = \begin{bmatrix} -1 & 1 & 0 \\ 1 & -1 & 0 \\ 0 & 0 & 2 \end{bmatrix}$$

there is no real invertible R, real strictly upper-triangular N, and real diagonal D with $L = R^{-1}NR + D$. (If $L = R^{-1}NR + D$, then

$$(L - D)^3 = \left(R^{-1}NR\right)^3 = R^{-1}N^3R = 0;$$

the three resulting equations in D_{11}, D_{22}, D_{33} have no simultaneous solution.)

Appendix B. Exponentials

In this section we review the matrix exponential and work several geologically relevant examples. References include Belinfante and Kolman (1972); Gilmore (1974); Curtis (1984); Hall (2003); Moler and Van Loan (2003); Pollatsek (2009).

In calculus, the exponential function $\exp x = e^x$ is described by the power series

$$\exp x = \sum_{k=0}^{\infty} \frac{1}{k!} x^k = 1 + x + \frac{1}{2}x^2 + \cdots.$$

Similarly, for any square matrix L we can define

$$\exp L = \sum_{k=0}^{\infty} \frac{1}{k!} L^k = I + L + \frac{1}{2}L^2 + \cdots.$$

This series converges for any L, so exp is a well-defined matrix exponential function. An important special case occurs when L is strictly upper-triangular or strictly lower-triangular; then $L^n = 0$ (where L is $n \times n$), so the series truncates after n terms. For example,

$$\exp \begin{bmatrix} 0 & L_{12} \\ 0 & 0 \end{bmatrix} = \begin{bmatrix} 1 & L_{12} \\ 0 & 1 \end{bmatrix}$$

and

$$\exp \begin{bmatrix} 0 & L_{12} & L_{13} \\ 0 & 0 & L_{23} \\ 0 & 0 & 0 \end{bmatrix} = \begin{bmatrix} 1 & L_{12} & L_{13} + \frac{1}{2}L_{12}L_{23} \\ 0 & 1 & L_{23} \\ 0 & 0 & 1 \end{bmatrix}.$$

The matrix exponential respects change of basis:

$$\exp PJP^{-1} = P(\exp J)P^{-1}$$

for any J and invertible P. This property greatly expedites computations, as follows. First, the Jordan blocks (see Appendix A) have simple exponentials:

$$\begin{aligned} \exp \begin{bmatrix} \lambda \end{bmatrix} &= \begin{bmatrix} e^\lambda \end{bmatrix}, \\ \exp \begin{bmatrix} \lambda & 1 \\ 0 & \lambda \end{bmatrix} &= \begin{bmatrix} e^\lambda & e^\lambda \\ 0 & e^\lambda \end{bmatrix}, \\ \exp \begin{bmatrix} \lambda & 1 & 0 \\ 0 & \lambda & 1 \\ 0 & 0 & \lambda \end{bmatrix} &= \begin{bmatrix} e^\lambda & e^\lambda & \frac{1}{2}e^\lambda \\ 0 & e^\lambda & e^\lambda \\ 0 & 0 & e^\lambda \end{bmatrix}. \end{aligned}$$

Second, the exponential function operates independently on each block in a Jordan matrix. For example,

$$\exp \begin{bmatrix} \lambda_1 & 1 & 0 \\ 0 & \lambda_1 & 0 \\ 0 & 0 & \lambda_2 \end{bmatrix} = \begin{bmatrix} e^{\lambda_1} & e^{\lambda_1} & 0 \\ 0 & e^{\lambda_1} & 0 \\ 0 & 0 & e^{\lambda_2} \end{bmatrix}.$$

So, we have a concrete algorithm for computing $\exp L$, for any matrix L: Find the Jordan decomposition $L = PJP^{-1}$, compute $\exp J$ using the examples above, and then reconstruct $\exp L = P(\exp J)P^{-1}$. This method is more appropriate for symbolic than for numerical calculation, because the Jordan canonical form is not numerically robust (see Moler and Van Loan (2003) for other methods of computing the exponential).

Here are some other properties enjoyed by the matrix exponential.

- $\exp 0 = I$, where 0 is the zero matrix.
- L and $\exp L$ commute, meaning $L(\exp L) = (\exp L)L$.
- If L_1 and L_2 commute, then

  $$\exp(L_1 + L_2) = (\exp L_1)(\exp L_2).$$

  If L_1 and L_2 do not commute, then the equation does not hold in general. There is a more general formula, called the Baker-Campbell-Hausdorff formula, that we do not discuss here.
- Whether or not L_1 and L_2 commute, the Trotter product formula (Trotter, 1959) states that

  $$\exp(L_1 + L_2) = \lim_{n\to\infty} \left(\exp\left(\frac{1}{n}L_1\right)\exp\left(\frac{1}{n}L_2\right)\right)^n.$$
- $(\exp L)^n = \exp nL$ for any integer n.
- If λ is an eigenvalue of L, then $\exp\lambda$ is an eigenvalue of $\exp L$, with the same eigenspace. In particular, if L has only real eigenvalues then $\exp L$ has only positive eigenvalues.
- The exponential of a symmetric matrix is symmetric. The exponential of an antisymmetric matrix is orthogonal.
- $\det(\exp L) = \exp(\mathrm{tr}L)$.

- If K is a matrix dependent on t and $\dot{K}K = K\dot{K}$, then

$$\frac{d}{dt}\exp K = \dot{K}(\exp K) = (\exp K)\dot{K}.$$

The final property listed above explains why $\vec{y} = (\exp tL)\vec{x}$ solves the differential equation (1). Given any L — even a time-dependent one — let

$$K = \int_0^t L(\tau)\, d\tau$$

be the component-wise antiderivative of L, such that $K(0)$ is the zero matrix. If $\dot{K} = L$ commutes with K, then $\vec{y} = (\exp K)\vec{x}$ solves $\dot{\vec{y}} = L\vec{y}$. This paper has simply focused on the case where L is constant, because it seems to be most geologically relevant. Provost et al. (2004) mention a slightly less-special case: when L is of the form $L(t) = f(t)L(0)$ for a scalar function f.

The matrix exponential is computed in *Mathematica* by `MatrixExp`, in *Maple* by `MatrixExponential`, and in *MATLAB* by `expm`.

We now work four increasingly sophisticated examples of using Eq. (2) to solve the differential equation (1). In each example we compute the Jordan decomposition of tL, exponentiate the Jordan matrix, and recombine. However, in many cases one can shortcut the process.

Appendix B.1. Simple shear

Two-dimensional simple shear has velocity gradient tensor

$$L = \begin{bmatrix} 0 & \dot{\gamma} \\ 0 & 0 \end{bmatrix}$$

for some constant $\dot{\gamma}$ that represents the shear strain rate. The matrix tL is strictly upper-triangular, so its exponential is easily computed:

$$\exp tL = \begin{bmatrix} 1 & t\dot{\gamma} \\ 0 & 1 \end{bmatrix}.$$

As t goes from 0 to 1, this tensor interpolates, in a natural way, between the identity and finite simple shear with off-diagonal entry $\dot{\gamma}$:

$$\exp L = \begin{bmatrix} 1 & \dot{\gamma} \\ 0 & 1 \end{bmatrix}.$$

In simple shear, it is common to denote the off-diagonal entry in L by $\dot{\gamma}$ and the off-diagonal entry in $F = \exp L$ by γ, but they are equal as long as the time scale is chosen so that deformation takes one unit of time.

Appendix B.2. Coaxial deformation

The velocity gradient tensor

$$L = \begin{bmatrix} \lambda_1 & 0 & 0 \\ 0 & \lambda_2 & 0 \\ 0 & 0 & \lambda_3 \end{bmatrix},$$

where the λ_i are arbitrary constants, describes a three-dimensional coaxial deformation. To compute the progressive deformation corresponding to L, we first multiply by t:

$$tL = \begin{bmatrix} t\lambda_1 & 0 & 0 \\ 0 & t\lambda_2 & 0 \\ 0 & 0 & t\lambda_3 \end{bmatrix}.$$

Then we compute the matrix exponential. For a diagonal matrix this is easy; we just exponentiate each diagonal entry:

$$\exp tL = \begin{bmatrix} {\mu_1}^t & 0 & 0 \\ 0 & {\mu_2}^t & 0 \\ 0 & 0 & {\mu_3}^t \end{bmatrix},$$

where $\mu_i = e^{\lambda_i}$. As t goes from 0 to 1, this tensor interpolates between the identity and the coaxial finite deformation tensor.

More generally, let L be any symmetric tensor. Then L diagonalizes as $L = QDQ^{-1}$, where Q is orthogonal. The deformation produced by L is coaxial, with stretching and shortening directions given by the column vectors of Q. The progressive deformation tensor is

$$\exp tL = \exp t\left(QDQ^{-1}\right) = Q(\exp tD)Q^{-1}.$$

Appendix B.3. Triclinic transpression

The triclinic transpression of Lin et al. (1998) is a more complicated deformation (see Fig. 1), described by the velocity gradient matrix

$$L = \begin{bmatrix} 0 & \dot{\gamma}\cos\phi & 0 \\ 0 & -\dot{\epsilon} & 0 \\ 0 & \dot{\gamma}\sin\phi & \dot{\epsilon} \end{bmatrix} \tag{B.1}$$

for some constants $\dot{\epsilon}$, $\dot{\gamma}$, ϕ. As always, the progressive deformation is $\vec{y} = (\exp tL)\vec{x}$; however, the details of how $\exp tL$ is computed depend somewhat on $\dot{\epsilon}$, $\dot{\gamma}$, and ϕ. In the typical and most geologically useful case, when $\dot{\epsilon} \neq 0$, tL is diagonalizable as

$$tL = P \begin{bmatrix} 0 & 0 & 0 \\ 0 & -t\dot{\epsilon} & 0 \\ 0 & 0 & t\dot{\epsilon} \end{bmatrix} P^{-1},$$

where

$$P = \begin{bmatrix} 1 & 2\dot{\gamma}\cos\phi & 0 \\ 0 & -2\dot{\epsilon} & 0 \\ 0 & \dot{\gamma}\sin\phi & 1 \end{bmatrix}.$$

We exponentiate the diagonal matrix and recombine as follows.

$$\exp tL = P \begin{bmatrix} 1 & 0 & 0 \\ 0 & e^{-t\dot{\epsilon}} & 0 \\ 0 & 0 & e^{t\dot{\epsilon}} \end{bmatrix} P^{-1}$$

$$= \begin{bmatrix} 1 & \frac{\dot{\gamma}}{\dot{\epsilon}}(1 - e^{-\dot{\epsilon}t})\cos\phi & 0 \\ 0 & e^{-\dot{\epsilon}t} & 0 \\ 0 & \frac{\dot{\gamma}}{\dot{\epsilon}}\sinh(\dot{\epsilon}t)\sin\phi & e^{\dot{\epsilon}t} \end{bmatrix}. \tag{B.2}$$

Eq. (B.2) agrees with Lin et al. (1998).

The special case of $\dot\epsilon = 0$ can be handled in the same way. The matrix tL may not be diagonalizable, but it can still be exponentiated in terms of its Jordan decomposition.

Appendix B.4. Upper-triangular deformation

For a final example, consider the upper-triangular deformation (Fig. 1) from Tikoff and Fossen (1993). It arises from a velocity gradient tensor of the form

$$L = \begin{bmatrix} \dot\epsilon_x & \dot\gamma_{xy} & \dot\gamma_{xz} \\ 0 & \dot\epsilon_y & \dot\gamma_{yz} \\ 0 & 0 & \dot\epsilon_z \end{bmatrix}.$$

If $\dot\epsilon_x$, $\dot\epsilon_y$, and $\dot\epsilon_z$ are distinct, then L is diagonalizable as

$$L = P \begin{bmatrix} \dot\epsilon_x & 0 & 0 \\ 0 & \dot\epsilon_y & 0 \\ 0 & 0 & \dot\epsilon_z \end{bmatrix} P^{-1},$$

where

$$P = \begin{bmatrix} 1 & \frac{-\dot\gamma_{xy}}{\dot\epsilon_x - \dot\epsilon_y} & \frac{\dot\gamma_{xy}\dot\gamma_{yz} + \dot\gamma_{xz}(\dot\epsilon_z - \dot\epsilon_y)}{(\dot\epsilon_x - \dot\epsilon_z)(\dot\epsilon_y - \dot\epsilon_z)} \\ 0 & 1 & \frac{-\dot\gamma_{yz}}{\dot\epsilon_y - \dot\epsilon_z} \\ 0 & 0 & 1 \end{bmatrix}.$$

The progressive deformation is given by

$$\exp tL = P \begin{bmatrix} e^{t\dot\epsilon_x} & 0 & 0 \\ 0 & e^{t\dot\epsilon_y} & 0 \\ 0 & 0 & e^{t\dot\epsilon_z} \end{bmatrix} P^{-1}$$

$$= \begin{bmatrix} e^{\dot\epsilon_x t} & \dot\gamma_{xy}\frac{e^{\dot\epsilon_x t} - e^{\dot\epsilon_y t}}{\dot\epsilon_x - \dot\epsilon_y} & \dot\gamma_{xz}\frac{e^{\dot\epsilon_x t} - e^{\dot\epsilon_z t}}{\dot\epsilon_x - \dot\epsilon_z} + a \\ 0 & e^{\dot\epsilon_y t} & \dot\gamma_{yz}\frac{e^{\dot\epsilon_y t} - e^{\dot\epsilon_z t}}{\dot\epsilon_y - \dot\epsilon_z} \\ 0 & 0 & e^{\dot\epsilon_z t} \end{bmatrix},$$

where for typographical convenience we have introduced the notation

$$\begin{aligned} a = & \frac{\dot\gamma_{xy}\dot\gamma_{yz} e^{\dot\epsilon_x t}}{(\dot\epsilon_x - \dot\epsilon_y)(\dot\epsilon_x - \dot\epsilon_z)} \\ & - \frac{\dot\gamma_{xy}\dot\gamma_{yz} e^{\dot\epsilon_y t}}{(\dot\epsilon_x - \dot\epsilon_y)(\dot\epsilon_y - \dot\epsilon_z)} \\ & + \frac{\dot\gamma_{xy}\dot\gamma_{yz} e^{\dot\epsilon_z t}}{(\dot\epsilon_x - \dot\epsilon_z)(\dot\epsilon_y - \dot\epsilon_z)}. \end{aligned}$$

If $\dot\epsilon_x$, $\dot\epsilon_y$, and $\dot\epsilon_z$ are not distinct, then tL may not be diagonalizable, but we can always compute its Jordan decomposition and exponentiate from there. There are several subcases. For example, when $\dot\epsilon_x = \dot\epsilon_y = \dot\epsilon_z$ (just call them $\dot\epsilon$) and $\dot\gamma_{xy}, \dot\gamma_{xz}, \dot\gamma_{yz} \neq 0$, the Jordan decomposition of tL is

$$tL = P \begin{bmatrix} t\dot\epsilon & 1 & 0 \\ 0 & t\dot\epsilon & 1 \\ 0 & 0 & t\dot\epsilon \end{bmatrix} P^{-1},$$

where

$$P = \begin{bmatrix} 1 & 0 & 0 \\ 0 & \frac{1}{t\dot\gamma_{xy}} & \frac{-\dot\gamma_{xz}}{t^2\dot\gamma_{xy}^2\dot\gamma_{yz}} \\ 0 & 0 & \frac{1}{t^2\dot\gamma_{xy}\dot\gamma_{yz}} \end{bmatrix}.$$

This implies that

$$\exp tL = \begin{bmatrix} e^{\dot\epsilon t} & \dot\gamma_{xy} t e^{\dot\epsilon t} & \dot\gamma_{xz} t e^{\dot\epsilon t} + a \\ 0 & e^{\dot\epsilon t} & \dot\gamma_{yz} t e^{\dot\epsilon t} \\ 0 & 0 & e^{\dot\epsilon t} \end{bmatrix},$$

where $a = \frac{1}{2}\dot\gamma_{xy}\dot\gamma_{yz} t^2 e^{\dot\epsilon t}$. These calculations agree with Tikoff and Fossen (1993).

Appendix C. Logarithms

In this section we review the matrix logarithm and work a few geologically relevant examples. Logarithms are subtle. Some matrices do not have logarithms, while others have more than one. To define a well-defined logarithm function, we must place restrictions on both F and $\ln F$.

If F is a square, real matrix, all of whose eigenvalues are either nonreal or positive (that is, there are no real eigenvalues less than or equal to 0), then there exists a unique real matrix L such that $\exp L = F$ and all eigenvalues of L have imaginary part in $(-\pi, \pi)$ (Kenney and Laub, 1989). We call this matrix L the *principal logarithm* of F, and denote it $\ln F$.

In particular, if all of the eigenvalues of F are real and positive, then $\ln F$ has only real eigenvalues. If, in addition, every eigenspace of F is one-dimensional, then $\ln F$ is the only real matrix that exponentiates to F (Culver, 1966, Theorem 2). This mathematical special case — a positive-eigenvalue F with one-dimensional eigenspaces — encompasses most finite deformation tensors of geological interest, including pure and simple shears and many combinations thereof, but excluding pure rotations. On the other hand, when some eigenspace of F has dimension greater than 1, this eigenspace can be exploited to produce other real L such that $\exp L = F$. An example is given below.

Now we describe how to compute principal logarithms. The power series for $\ln(1 + x)$ gives us a matrix power series

$$\begin{aligned} \ln(I + N) &= \sum_{k=1}^{\infty} \frac{(-1)^{k+1}}{k} N^k \\ &= N - \frac{1}{2}N^2 + \frac{1}{3}N^3 - \cdots. \end{aligned}$$

This immediately yields logarithms for certain simple shear matrices — those of the form $I + N$, with N strictly upper-triangular:

$$\ln \begin{bmatrix} 1 & N_{12} \\ 0 & 1 \end{bmatrix} = \begin{bmatrix} 0 & N_{12} \\ 0 & 0 \end{bmatrix},$$

$$\ln \begin{bmatrix} 1 & N_{12} & N_{13} \\ 0 & 1 & N_{23} \\ 0 & 0 & 1 \end{bmatrix}$$

$$= \begin{bmatrix} 0 & N_{12} & N_{13} - \frac{1}{2}N_{12}N_{23} \\ 0 & 0 & N_{23} \\ 0 & 0 & 0 \end{bmatrix}.$$

A Jordan block with eigenvalue μ can be written in the form $\mu(I+N)$, where $I+N$ is of the form just discussed. Its logarithm is then $(\ln\mu)I + \ln(I+N)$. Here are the crucial examples.

$$\begin{aligned}
\ln\begin{bmatrix} \mu \end{bmatrix} &= \begin{bmatrix} \ln\mu \end{bmatrix}, \\
\ln\begin{bmatrix} \mu & 1 \\ 0 & \mu \end{bmatrix} &= \begin{bmatrix} \ln\mu & \frac{1}{\mu} \\ 0 & \ln\mu \end{bmatrix}, \\
\ln\begin{bmatrix} \mu & 1 & 0 \\ 0 & \mu & 1 \\ 0 & 0 & \mu \end{bmatrix} &= \begin{bmatrix} \ln\mu & \frac{1}{\mu} & \frac{-1}{2\mu^2} \\ 0 & \ln\mu & \frac{1}{\mu} \\ 0 & 0 & \ln\mu \end{bmatrix}.
\end{aligned}$$

Because the matrix exponential respects Jordan blocks and change of basis, so must its inverse the matrix logarithm. For any positive-eigenvalue Jordan matrix J, compute $\ln J$ by taking logarithms of its Jordan blocks individually. For any positive-eigenvalue matrix F, compute $\ln F$ via its Jordan decomposition $F = PJP^{-1}$:

$$\ln PJP^{-1} = P(\ln J)P^{-1}.$$

As long as F has only positive eigenvalues and only real P are used in the Jordan decomposition, this construction produces a well-defined matrix logarithm $\ln F$ satisfying the following properties:

- $\exp(\ln F) = F$.
- $\ln(\exp L) = L$ for any real-eigenvalue L.
- If $\mu > 0$ is an eigenvalue of F, then $\ln\mu$ is an eigenvalue of $\ln F$ with the same eigenspace. In particular, $\ln F$ has only real eigenvalues.
- F and $\ln F$ commute.
- If $\ln F_1$ and $\ln F_2$ commute, then

$$\ln(F_1F_2) = \ln F_1 + \ln F_2.$$

Matrix logarithms are computed in *MATLAB* by `logm` and in *Maple* by `MatrixFunction`. *Mathematica* comes with no built-in matrix logarithm function. Appendix F gives *Mathematica* code for computing logarithms via the Jordan decomposition.

We now work three geologically relevant examples, using matrix logarithms to compute the velocity gradient tensor L from the finite deformation tensor F. The basic process is to compute the Jordan decomposition of $F = PJP^{-1}$, then the principal logarithm $\ln J$, then the product $L = P(\ln J)P^{-1}$.

Appendix C.1. Simple shear

Consider the two-dimensional simple shear

$$F = \begin{bmatrix} 1 & \gamma \\ 0 & 1 \end{bmatrix}.$$

Its principal logarithm is

$$\ln F = \begin{bmatrix} 0 & \gamma \\ 0 & 0 \end{bmatrix}.$$

In fact, this matrix is the only real logarithm of F. It leads to the progressive simple shear matrix

$$\exp(t\ln F) = \begin{bmatrix} 1 & t\gamma \\ 0 & 1 \end{bmatrix},$$

which at time $t = 1$ equals F. These calculations agree with the simple shear example in Appendix B.

Appendix C.2. Coaxial deformation

Let

$$F = \begin{bmatrix} \mu_1 & 0 & 0 \\ 0 & \mu_2 & 0 \\ 0 & 0 & \mu_3 \end{bmatrix}$$

(with $\mu_1, \mu_2, \mu_3 > 0$) be a coaxial finite deformation tensor. Because it is diagonal, its principal logarithm is easy to compute:

$$\ln F = \begin{bmatrix} \ln\mu_1 & 0 & 0 \\ 0 & \ln\mu_2 & 0 \\ 0 & 0 & \ln\mu_3 \end{bmatrix}.$$

If the μ_i are distinct, then this matrix is the only real logarithm of F. Taking it as our velocity gradient tensor, we obtain a progressive deformation tensor

$$\exp(t\ln F) = \begin{bmatrix} {\mu_1}^t & 0 & 0 \\ 0 & {\mu_2}^t & 0 \\ 0 & 0 & {\mu_3}^t \end{bmatrix},$$

which interpolates the coaxial finite deformation in a natural way.

Continuing this coaxial example, consider the special case of $\mu_1 = \mu_2$. Now the tensor F has an eigenvalue with a two-dimensional eigenspace, which provides room for infinitely many logarithms, as follows. For any integer k, let

$$L_k = \begin{bmatrix} \ln\mu_1 & -2k\pi & 0 \\ 2k\pi & \ln\mu_1 & 0 \\ 0 & 0 & \ln\mu_3 \end{bmatrix}. \tag{C.1}$$

Fig. 4 illustrates L_k for $k = 0, 1$. For every integer k, $\exp L_k = F$. Thus F has infinitely many real logarithms. (There are even more logarithms of F than these. See Appendix F and Gantmacher (1959, p. 239) for a complete description.) The progressive deformation tensor

$$\exp tL_k = \begin{bmatrix} {\mu_1}^t\cos(t2k\pi) & -{\mu_1}^t\sin(t2k\pi) & 0 \\ {\mu_1}^t\sin(t2k\pi) & {\mu_1}^t\cos(t2k\pi) & 0 \\ 0 & 0 & {\mu_3}^t \end{bmatrix}$$

resulting from L_k rotates space k times about the x_3-axis, but this extraneous rotation is undetectable in the finite deformation, which for all k is the same $\vec{y} = F\vec{x}$. Among all of the progressive deformations $\vec{y} = (\exp tL_k)\vec{x}$, the "simplest" is the one with no extraneous rotation; it is the one arising from L_0, which is the only L_k with only real eigenvalues, and which equals the principal logarithm $\ln F$ (see Fig. 4a).

Appendix C.3. Upper-triangular deformation

Finally, suppose that we have an arbitrary upper-triangular finite deformation

$$F = \begin{bmatrix} F_{11} & F_{12} & F_{13} \\ 0 & F_{22} & F_{23} \\ 0 & 0 & F_{33} \end{bmatrix}$$

and that we want to infer the corresponding progressive deformation. We first compute the Jordan decomposition; in the typical case, when F_{11}, F_{22}, and F_{33} are distinct, the decomposition is

$$F = P \begin{bmatrix} F_{11} & 0 & 0 \\ 0 & F_{22} & 0 \\ 0 & 0 & F_{33} \end{bmatrix} P^{-1},$$

where

$$P = \begin{bmatrix} 1 & \frac{-F_{12}}{F_{11}-F_{22}} & \frac{-F_{13}F_{22}+F_{12}F_{23}+F_{13}F_{33}}{(F_{11}-F_{33})(F_{22}-F_{33})} \\ 0 & 1 & \frac{-F_{23}}{F_{22}-F_{33}} \\ 0 & 0 & 1 \end{bmatrix}.$$

Then we compute the progressive deformation tensor

$$\exp(t \ln F) = P \begin{bmatrix} {F_{11}}^t & 0 & 0 \\ 0 & {F_{22}}^t & 0 \\ 0 & 0 & {F_{33}}^t \end{bmatrix} P^{-1}$$

$$= \begin{bmatrix} {F_{11}}^t & F_{12}\frac{{F_{11}}^t-{F_{22}}^t}{F_{11}-F_{22}} & F_{13}\frac{{F_{11}}^t-{F_{33}}^t}{F_{11}-F_{33}} + a \\ 0 & {F_{22}}^t & F_{23}\frac{{F_{22}}^t-{F_{33}}^t}{F_{22}-F_{33}} \\ 0 & 0 & {F_{33}}^t \end{bmatrix},$$

where for typographical convenience we have introduced the notation

$$\begin{aligned} a = & \frac{F_{12}F_{23}{F_{11}}^t}{(F_{11}-F_{22})(F_{11}-F_{33})} \\ & + \frac{F_{12}F_{23}{F_{22}}^t}{(F_{22}-F_{11})(F_{22}-F_{33})} \\ & + \frac{F_{12}F_{23}{F_{33}}^t}{(F_{33}-F_{11})(F_{33}-F_{22})}. \end{aligned}$$

The reader can verify that this matrix equals I when $t = 0$ and F when $t = 1$.

Appendix D. Powers and roots

Let F be a positive-eigenvalue matrix, or indeed any matrix for which the principal logarithm $\ln F$ is defined. For any real number t, define the matrix power F^t by

$$F^t = \exp(t \ln F).$$

It is easily seen to satisfy these properties:

- For any integer k, F^k agrees with its usual definition as the repeated product of F with itself k times.
- $t \ln F = \ln(F^t)$.
- $F^t F^s = F^{t+s}$.
- $(F^t)^s = F^{ts}$.
- $\frac{d}{dt}F^t = (\ln F)F^t = F^t(\ln F)$.

For any positive integer n, we can define the (principal) nth root of F as

$$\sqrt[n]{F} = F^{1/n} = \exp\left(\frac{1}{n}\ln F\right).$$

It satisfies $\left(\sqrt[n]{F}\right)^n = F$, but it is not the only matrix whose nth power is F. For example, the 2×2 identity matrix I has at least four square roots, because

$$\begin{bmatrix} \pm 1 & 0 \\ 0 & \pm 1 \end{bmatrix}^2 = \begin{bmatrix} 1 & 0 \\ 0 & 1 \end{bmatrix},$$

but the principal square root is $\sqrt{I} = I$.

Matrix powers are computed in *Mathematica* and *Maple* by `MatrixPower` and in *MATLAB* using the syntax `F^t` (see also `sqrtm` and `funm`).

Appendix E. Miscellaneous calculations

In this section, we compute two expressions for the kinematic vorticity W_k (Section 4.9) that do not commonly appear in the structural geology literature. Both computations require this fact from linear algebra: For any (real, 3×3) matrix A with eigenvalues α_1, α_2, α_3,

$$\operatorname{tr} A^2 = {\alpha_1}^2 + {\alpha_2}^2 + {\alpha_3}^2.$$

To see this, let $A = PJP^{-1}$ be the complex Jordan decomposition of A (see Appendix A). Then J is upper-triangular with diagonal entries α_1, α_2, α_3, and so

$$\begin{aligned} \operatorname{tr} A^2 &= \operatorname{tr} PJ^2P^{-1} = \operatorname{tr} J^2 \\ &= {\alpha_1}^2 + {\alpha_2}^2 + {\alpha_3}^2. \end{aligned}$$

We also need the *Frobenius norm* $|A|$ of A, which is defined as

$$|A| = \sqrt{\operatorname{tr} A^\top A} = \sqrt{\sum_{i=1}^{3}\sum_{j=1}^{3} {A_{ij}}^2}.$$

The kinematic vorticity is commonly (e.g., Means et al., 1980; Xypolias, 2010) defined as

$$W_k = \frac{w}{\sqrt{2({s_1}^2 + {s_2}^2 + {s_3}^2)}},$$

where the s_i are the eigenvalues of the stretching tensor S. From this definition and the definition of the vorticity w (Section 4.8) it follows that

$$W_k^2 = \frac{2\left({W_{32}}^2 + {W_{13}}^2 + {W_{21}}^2\right)}{{s_1}^2 + {s_2}^2 + {s_3}^2}.$$

The numerator equals $|W|^2$, while the denominator equals $\operatorname{tr} S^2 = \operatorname{tr} S^\top S = |S|^2$. Thus $W_k^2 = |W|^2/|S|^2$ and $W_k = |W|/|S|$, as claimed in Section 4.9.

The identity $W_k^2 = |W|^2/|S|^2$ also implies that

$$W_k = \sqrt{1 - 1 + \frac{|W|^2}{|S|^2}} = \sqrt{1 - \frac{|S|^2 - |W|^2}{|S|^2}}.$$

Using $L = S + W$, $S^\top = S$, and $W^\top = -W$, it is not difficult to show that

$$\begin{aligned} \operatorname{tr} L^2 &= \operatorname{tr} S^2 + \operatorname{tr} SW + \operatorname{tr} WS + \operatorname{tr} W^2 \\ &= \operatorname{tr} S^\top S - \operatorname{tr} W^\top W \\ &= |S|^2 - |W|^2. \end{aligned}$$

But $\operatorname{tr} L^2 = {\lambda_1}^2 + {\lambda_2}^2 + {\lambda_3}^2$, where the λ_i are the eigenvalues of L. Combining these facts, we have

$$W_k = \sqrt{1 - \frac{{\lambda_1}^2 + {\lambda_2}^2 + {\lambda_3}^2}{|S|^2}},$$

as claimed in Section 4.9.